PROCEEDINGS A

royalsocietypublishing.org/journal/rspa

Research

Cite this article: Magda G, Charkaluk E, Triantafyllidis N. 2024 Forces in interacting ferromagnetic conductors subjected to electrical currents and magnetic fields. *Proc. R. Soc. A* **480**: 20230691.
https://doi.org/10.1098/rspa.2023.0691

Received: 21 September 2023
Accepted: 2 May 2024

Subject Areas:
mechanical engineering, electrical engineering, structural engineering

Keywords:
continuum mechanics, coupled mechanical and electromagnetic processes, magnetoelasticity, variational principle, finite elements

Author for correspondence:
Nicolas Triantafyllidis
e-mail:
nicolas.triantafyllidis@polytechnique.edu

THE ROYAL SOCIETY
PUBLISHING

Forces in interacting ferromagnetic conductors subjected to electrical currents and magnetic fields

Geoffrey Magda[1], Eric Charkaluk[1,2] and Nicolas Triantafyllidis[1,2,3]

[1]Laboratoire de Mécanique des Solides (CNRS UMR 7649), Ecole Polytechnique, Institut Polytechnique de Paris, Palaiseau, France
[2]Département de Mécanique, École Polytechnique, Route de Saclay, Palaiseau 91128, France
[3]Aerospace Engineering Department & Mechanical Engineering Department (emeritus), The University of Michigan, Ann Arbor, MI 48109-2140, USA

NT, 0000-0002-1885-8887

We revisit the classical problem of Lorentz forces exerted on conductors subjected simultaneously to electrical currents and external magnetic fields within the framework of magnetostatics, i.e. when all field quantities are time-independent. In contrast to the well-known results pertaining to non-magnetic materials, we consider here ferromagnetic materials and study the influence of the magnetic constitutive law on the forces exerted on these conductors. Following the general setting for the coupled magnetoelastic boundary value problem in three dimensions (Lagrangian and Eulerian descriptions), we restrict attention to the two-dimensional problem of a single, two or many interacting parallel conductors of infinite extent and circular sections. Both analytical and numerical (FEM) results are presented. For a single conductor, where the magnetic properties do not influence the force exerted, we calculate the magnetization and magnetic stress fields; analytically for the linear magnetic response and numerically for the general nonlinear case with saturation. For two parallel conductors, the magnetic properties affect significantly the Lorentz forces when the conductors are placed close to each other, as the magnetic fields outside them are strongly influenced by the conductors' magnetic response. For the case of an infinite array of parallel conductors, there is no influence of their magnetic properties on the Lorentz

© 2024 The Author(s) Published by the Royal Society. All rights reserved.

forces when same direction currents are applied, while only a small magnetic effect is found for currents applied in alternating directions, even for closely spaced conductors.

royalsocietypublishing.org/journal/rspa Proc. R. Soc. A 480: 20230691

1. Introduction

We revisit the problem of Lorentz forces on electrical current-carrying conductors subjected to a remote magnetic field, a classical topic in magnetostatics (the study of magnetic systems where all field quantities are time-independent). The novel element here is the influence of the conductors' magnetic properties on these forces. The case of a single conductor has been discussed by [1], who shows that the Lorentz force/unit length is independent of the magnetic properties and the shape of the conductor, for the case of a conductor placed in a uniform external magnetic field perpendicular to its axis. The same result is obtained by [2], who in addition presents some careful experiments to back this theoretical result.

From previous work pertaining to the Lorentz forces between magnetizable wires, of some relevance to our study is the work in [3], who treat magnetizable nano-wires embedded in materials but those wires do not carry electric currents and the Lorentz forces are not considered. The mechanical behaviour and stability of a current-carrying wire array has been studied for the development of Z-pinch structures in [4], who do not consider magnetization of the wires, but focus on stability and thermal effects. The influence of magnetic constitutive law on the Lorentz forces between two or more (periodic array) parallel conductors subjected simultaneously to a uniform external magnetic field and a current density has received considerably less attention to the best of the authors' knowledge and is the purpose of this investigation. An additional motivation for our work pertains to composites consisting of ferromagnetic rods inside an elastomeric matrix (e.g. [5]), although no electrical currents were considered there, thus motivating the study of an array of current-carrying conductors presented here in §4b,c.

To study the problem in the most general setting, we start with the variational derivation of the magnetic and mechanical governing equations, which requires a Lagrangian (reference configuration) approach (see [6,7]) to determine the Maxwell (vacuum) and total (inside the conductor) stress fields. The theory is presented in its most general version allowing for finite strains in the conductor (in the case when a mechanically soft conducting material is considered). However, due to the small strains in the applications of interest that pertain to metallic conductors, the Eulerian (current configuration) version of the governing equations is used to obtain the magnetic field vector and the magnetic component of the stress tensor which are of interest here. For reasons of completeness of the presentation and to provide a consistent methodology for simultaneously obtaining both mechanical and magnetic field quantities in a more general setting, both versions of the governing equations and boundary conditions are recorded. Of the two different methodologies to obtain the governing equations of the mechanical-electromagnetic boundary value problem, i.e. direct and variational, we choose here the latter since it is also the one used for the numerical (FEM) calculations. The main interest here is the calculation of the Lorentz forces between ferromagnetic conductors subjected to time-independent remote magnetic fields and electric currents. There are several methods for obtaining these forces, and the interested reader can find an extensive review in [8].

The outline of the presentation is as follows: after the motivation in §1 comes the general variational theory of the eddy current approximation in §2. The stresses are subsequently simplified for the case of small strains but arbitrary magnetic fields and the resulting theory is applied to the analytically tractable case of a single conductor with linear magnetic response subjected to an electric current and a magnetic field. We subsequently present an efficient way to calculate the total force on a conductor using the Maxwell tensor and a contour integral in the vacuum surrounding the conductor of interest.

The numerical implementation is given in §3 followed by the applications in §4. For a single conductor, where the magnetic properties do not influence the force exerted, we calculate the

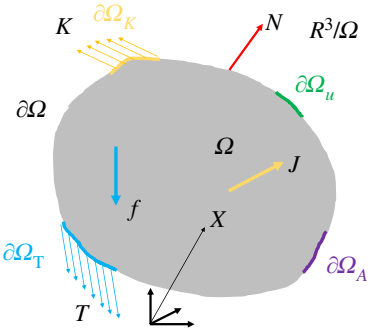

Figure 1. Schematics of the boundary value problem (reference configuration). Conductor occupies domain $\Omega \subset \mathbb{R}^3$ while a magnetic field exists in the entire space $\mathbb{R}^3$.

magnetization and magnetic stress fields. For two parallel conductors the magnetic properties affect significantly the Lorentz forces when the conductors are placed close to each other, as the magnetic fields outside them are strongly influenced by the conductors' magnetic response. For the case of an infinite array of parallel conductors, there is no influence of their magnetic properties on the Lorentz forces when same direction currents are applied while only a small magnetic effect is found for currents applied in alternating directions, even for closely spaced conductors. Conclusion is presented in §5.

2. Theory

Coordinate-free (dyadic) continuum mechanics notation is used with bold symbols referring to tensors and script ones to scalars; all field quantities are functions of the reference position $\boldsymbol{X}$ and when appropriate on time t. Lagrangian field quantities are denoted by capital letters, e.g. magnetic vector potential $\boldsymbol{A}$, magnetic field vector $\boldsymbol{B}$, h-field vector $\boldsymbol{H}$, current density $\boldsymbol{J}$, first Piola–Kirchhoff stress $\boldsymbol{\Pi}$, while their corresponding Eulerian counterparts are denoted by script letters, e.g. magnetic vector potential $\boldsymbol{a}$, magnetic field vector $\boldsymbol{b}$, h-field vector $\boldsymbol{h}$, current density $\boldsymbol{j}$, Cauchy stress $\boldsymbol{\sigma}$.[1] Moreover, the gradient operator ∇ is defined with respect to the reference configuration, i.e. $\nabla \equiv \partial/\partial \boldsymbol{X}$, while its current configuration counterpart is $\nabla \equiv \partial/\partial \boldsymbol{x}$.

(a) Variational approach

The schematics of the general boundary value problem are given in figure 1. The solid occupies a volume $\Omega \subset \mathbb{R}^3$ in the reference configuration with boundary $\partial\Omega$ and an outward normal $\boldsymbol{N}$. The solid is subjected to a reference current density $\boldsymbol{J}$ and an externally applied mechanical body force (per unit mass) $\boldsymbol{f}$. On the boundary, we apply a mechanical traction $\boldsymbol{T}$ and a current sheet $\boldsymbol{K}$ (per unit reference surface area). Surface tractions are applied on part of the boundary $\partial\Omega_T$ and the current sheet on part of the boundary $\partial\Omega_K$; displacement $\boldsymbol{u}$ and magnetic vector potential $\boldsymbol{A}$[2] can also be applied on parts of the boundary $\partial\Omega_u$ and $\partial\Omega_A$, respectively.

Neglecting the electric charge and the electric field energy contributions, the reference configuration *Lagrangian density* $\mathscr{\ell}$ (per unit reference volume) for the eddy current approximation (see [7]) is given by

$$\mathscr{\ell} \equiv -\frac{1}{2\mu_0 J}\boldsymbol{B}\cdot\boldsymbol{C}\cdot\boldsymbol{B} + \boldsymbol{J}\cdot\boldsymbol{A} - \rho_0\psi(\boldsymbol{C},\boldsymbol{B}) + \frac{1}{2}\rho_0(\dot{\boldsymbol{u}}\cdot\dot{\boldsymbol{u}}) + \rho_0\boldsymbol{f}\cdot\boldsymbol{u}; \quad \boldsymbol{B} \equiv \nabla \times \boldsymbol{A},\ \boldsymbol{C} \equiv \boldsymbol{F}^T\cdot\boldsymbol{F}, \tag{2.1}$$

[1]The capital-script letter rule is not applicable to field quantities relating the two configurations, where no ambiguity is possible and hence the usual standard notation is adopted, i.e. $\boldsymbol{F}$ for the deformation gradient or $\boldsymbol{u}$ for the displacement field.

[2]The Dirichlet condition in magnetics consists of prescribing $\boldsymbol{N} \times \boldsymbol{A}$.

where $\boldsymbol{B}$ is the reference magnetic field, $\boldsymbol{A}$ the reference magnetic vector potential,[3] $\psi(\boldsymbol{C},\boldsymbol{B})$[4] the specific (per unit mass) Helmholtz free energy and $\boldsymbol{C}$ the right Cauchy–Green tensor, expressed in terms of the deformation gradient $\boldsymbol{F}$. Following standard notation, ρ_0 is the reference mass density of the solid and $\dot{\boldsymbol{u}}$ denotes the time-derivative (velocity) of the displacement $\boldsymbol{u}$. Moreover, μ_0 is the magnetic permeability of vacuum and $J=\det\boldsymbol{F}$ denotes the deformation-induced volume change.

Based on (2.1), the reference configuration *total Lagrangian* $\mathscr{L}$ of the system becomes[5]

$$\mathscr{L}\equiv\int_{\mathbb{R}^3}\ell\,\mathrm{d}V+\int_{\partial\Omega}[\boldsymbol{T}\cdot\boldsymbol{u}+\boldsymbol{K}\cdot\boldsymbol{A}]\,\mathrm{d}S. \tag{2.2}$$

We also generalize the reference mass density ρ_0 in the definition of the Lagrangian density ℓ in (2.1) over the entire space $\mathbb{R}^3$ as follows: $\rho_0(\boldsymbol{X})\neq 0$ for $\boldsymbol{X}\in\Omega$ and $\rho_0(\boldsymbol{X})=0$ for $\boldsymbol{X}\in\mathbb{R}^3\backslash\Omega$. Integration over $\mathbb{R}^3$ is necessary to account for the magnetic field in both the body Ω and its surrounding space $\mathbb{R}^3\backslash\Omega$.

We proceed with the definition of the *action integral* $\mathscr{F}(\boldsymbol{A},\boldsymbol{u})$, obtained by integration of the Lagrangian $\mathscr{L}$ in (2.2) between arbitrary times t_1 and t_2. By Hamilton's principle, it is stationary

$$\mathscr{F}(\boldsymbol{A},\boldsymbol{u})\equiv\int_{t_1}^{t_2}\mathscr{L}\,\mathrm{d}t,\quad \delta\mathscr{F}=0;\ \delta\boldsymbol{A}(t_i)=\delta\boldsymbol{u}(t_i)=\boldsymbol{0},\ i=1,2\Longrightarrow\mathscr{F}_{,\boldsymbol{A}}[\delta\boldsymbol{A}]=\mathscr{F}_{,\boldsymbol{u}}[\delta\boldsymbol{u}]=0. \tag{2.3}$$

Consequently, the corresponding variations with respect to the independent variables $\boldsymbol{A}$ and $\boldsymbol{u}$ yield, respectively, the magnetic and mechanical governing equations and interface/boundary conditions.

(i) Magnetics equations: variations with respect to magnetic vector potential $\boldsymbol{A}$

Lagrangian version. Following (2.3), setting to zero the variation of $\mathscr{F}$ with respect to $\boldsymbol{A}$ one obtains

$$\mathscr{F}_{,\boldsymbol{A}}[\delta\boldsymbol{A}]=\int_{t_1}^{t_2}\left\{\int_{\mathbb{R}^3}\left[\boldsymbol{J}\cdot\delta\boldsymbol{A}-\frac{1}{\mu_0}(\boldsymbol{B}\cdot\boldsymbol{C})\cdot(\nabla\times\delta\boldsymbol{A})-\rho_0\frac{\partial\psi}{\partial\boldsymbol{B}}\cdot(\nabla\times\delta\boldsymbol{A})\right]\mathrm{d}V+\int_{\partial\Omega}[\boldsymbol{K}\cdot\delta\boldsymbol{A}]\mathrm{d}S\right\}\mathrm{d}t=0. \tag{2.4}$$

The domain $\mathbb{R}^3$ is separated into the volume Ω occupied by the body and the surrounding space $\mathbb{R}^3\backslash\Omega$. Taking into account the discontinuity of ρ_0 across $\partial\Omega$, integration by parts of (2.4) yields

$$\mathscr{F}_{,\boldsymbol{A}}[\delta\boldsymbol{A}]=\int_{t_1}^{t_2}\left\{\int_{\mathbb{R}^3}[(\boldsymbol{J}-\nabla\times\boldsymbol{H})\cdot\delta\boldsymbol{A}]\,\mathrm{d}V+\int_{\partial\Omega}[(\boldsymbol{K}-\boldsymbol{N}\times[\![\boldsymbol{H}]\!])\cdot\delta\boldsymbol{A}]\,\mathrm{d}S\right\}\mathrm{d}t=0, \tag{2.5}$$

where $\boldsymbol{H}$ is the reference configuration *h-field vector* (see [9]) and is given by

$$\boldsymbol{H}\equiv-\frac{\partial\ell}{\partial\boldsymbol{B}}=\begin{cases}\rho_0\dfrac{\partial\psi}{\partial\boldsymbol{B}}+\dfrac{1}{\mu_0 J}\boldsymbol{C}\cdot\boldsymbol{B}; & \forall\,\boldsymbol{X}\in\Omega,\\[2ex] \dfrac{1}{\mu_0 J}\boldsymbol{C}\cdot\boldsymbol{B}; & \forall\,\boldsymbol{X}\in\mathbb{R}^3\backslash\Omega.\end{cases} \tag{2.6}$$

The arbitrariness of $\delta\boldsymbol{A}$, (2.6) implies the following differential equation and boundary/interface condition

$$\nabla\times\boldsymbol{H}=\boldsymbol{J};\quad\forall\,\boldsymbol{X}\in\mathbb{R}^3,\quad \boldsymbol{N}\times[\![\boldsymbol{H}]\!]=\boldsymbol{K};\ \forall\,\boldsymbol{X}\in\partial\Omega, \tag{2.7}$$

where one recognizes the reference configuration Maxwell–Ampère Law in the eddy current approximation.

[3]An additional condition is needed for a unique $\boldsymbol{A}$, termed *gauge condition*; Coulomb gauge $\nabla\cdot\boldsymbol{A}=0$ is a typical choice.

[4]Dissipative phenomena (e.g. magnetic hysteresis or plasticity) are ignored and thus no internal variables are needed in ψ. Temperature dependence is ignored as well. The specific free energy used here depends on $(\boldsymbol{C},\boldsymbol{B}=J\boldsymbol{F}^{-1}\cdot\boldsymbol{b})$, as opposed to $(\boldsymbol{C},\boldsymbol{b}\cdot\boldsymbol{F})$ in [9–12]. Our choice, motivated by the fact that $\boldsymbol{B}$ is the Lagrangian counterpart of Eulerian $\boldsymbol{b}$, still complies with the angular momentum balance argument made in [12]. For a detailed explanation of this point, see [9].

[5]Without loss of generality, we can define the applied mechanical traction $\boldsymbol{T}$ and current sheet $\boldsymbol{K}$ on the entire boundary and impose a zero value when applicable.

To the above governing equation and boundary condition for $\boldsymbol{H}$, one should also add its counterpart for the reference configuration magnetic field vector $\boldsymbol{B}$, a consequence of (2.1)

$$\nabla\cdot\boldsymbol{B}=\boldsymbol{0};\quad \forall\boldsymbol{X}\in\mathbb{R}^3,\quad \boldsymbol{N}\cdot[\![\boldsymbol{B}]\!]=\boldsymbol{0};\quad \forall\boldsymbol{X}\in\partial\Omega,\quad (\boldsymbol{B}=\nabla\times\boldsymbol{A}). \tag{2.8}$$

Eulerian version. The reference configuration h-field vector, magnetic vector potential and field and current sheet are related via the deformation gradient $\boldsymbol{F}$ to their current configuration counterparts by (e.g. [13])

$$\boldsymbol{A}=\boldsymbol{a}\cdot\boldsymbol{F},\quad \boldsymbol{H}=\boldsymbol{h}\cdot\boldsymbol{F},\quad \boldsymbol{B}=J\boldsymbol{F}^{-1}\cdot\boldsymbol{b},\quad \boldsymbol{K}=J\boldsymbol{F}^{-1}\cdot\boldsymbol{\kappa}. \tag{2.9}$$

Consequently, the current configuration version of the magnetic constitutive relation (2.6) gives

$$\boldsymbol{h}=\begin{cases}\rho_0\dfrac{\partial\psi}{\partial\boldsymbol{B}}\cdot\boldsymbol{F}^{-1}+\dfrac{\boldsymbol{b}}{\mu_0}; & \forall\boldsymbol{x}\in\omega,\\[2ex] \dfrac{\boldsymbol{b}}{\mu_0}; & \forall\boldsymbol{x}\in\mathbb{R}^3\backslash\omega,\end{cases} \tag{2.10}$$

and the current configuration version counterpart of (2.7) becomes

$$\nabla\times\boldsymbol{h}=\boldsymbol{j};\quad \forall\boldsymbol{x}\in\mathbb{R}^3,\quad \boldsymbol{n}\times[\![\boldsymbol{h}]\!]=\boldsymbol{\kappa};\ \forall\boldsymbol{x}\in\partial\omega, \tag{2.11}$$

while the current configuration version counterpart of (2.8) is

$$\nabla\cdot\boldsymbol{b}=\boldsymbol{0};\ \forall\boldsymbol{x}\in\mathbb{R}^3,\qquad \boldsymbol{n}\cdot[\![\boldsymbol{b}]\!]=\boldsymbol{0};\ \forall\boldsymbol{x}\in\partial\omega,\quad (\boldsymbol{b}=\nabla\times\boldsymbol{a}), \tag{2.12}$$

where ω is the current configuration domain of the conductor, $\partial\omega$ its boundary and $\boldsymbol{n}$ its outward normal.

To equations (2.10)–(2.12) governing the magnetic response of a conductor, we must add the constitutive relation for the magnetization vector field $\boldsymbol{m}$, which is defined in the reference configuration and follows from (2.10)

$$\boldsymbol{b}=\mu_0(\boldsymbol{h}+\boldsymbol{m});\ \forall\boldsymbol{x}\in\mathbb{R}^3,\quad \boldsymbol{m}=-\rho_0\frac{\partial\psi}{\partial\boldsymbol{B}}\cdot\boldsymbol{F}^{-1};\ \forall\boldsymbol{x}\in\omega,\quad \boldsymbol{m}=\boldsymbol{0};\ \forall\boldsymbol{x}\in\mathbb{R}^3\backslash\omega. \tag{2.13}$$

(ii) Mechanics equations: variations with respect to displacement $\boldsymbol{u}$

Lagrangian version. Once again, from Hamilton's principle (2.3), setting to zero the variation of $\mathscr{F}$ with respect to $\boldsymbol{u}$ gives

$$\begin{aligned}\mathscr{F}_{,\boldsymbol{u}}[\delta\boldsymbol{u}]=\int_{t_1}^{t_2}\Bigg\{\int_{\mathbb{R}^3}\Bigg[&\left(\frac{1}{\mu_0 J}\left(\frac{1}{2}(\boldsymbol{B}\cdot\boldsymbol{C}\cdot\boldsymbol{B})\boldsymbol{I}-\boldsymbol{B}(\boldsymbol{C}\cdot\boldsymbol{B})\right)\cdot\boldsymbol{F}^{-1}-\rho_0\left(\frac{\partial\psi}{\partial\boldsymbol{C}}\right)\cdot\boldsymbol{F}^{T}\right):(\nabla\delta\boldsymbol{u})\\&+\rho_0\dot{\boldsymbol{u}}\cdot\frac{\mathrm{d}}{\mathrm{d}t}(\delta\boldsymbol{u})+\rho_0\boldsymbol{f}\cdot\delta\boldsymbol{u}\Bigg]\,\mathrm{d}V+\int_{\partial\Omega}[\boldsymbol{T}\cdot\delta\boldsymbol{u}]\,\mathrm{d}S\Bigg\}\,\mathrm{d}t=0.\end{aligned} \tag{2.14}$$

As before, the domain $\mathbb{R}^3$ is separated into the volume Ω occupied by the body and the surrounding space $\mathbb{R}^3\backslash\Omega$. Taking into account the discontinuity of ρ_0 across $\partial\Omega$, integration by parts of (2.14) in the space and the time domains (recalling also the end conditions at t_1, t_2 in (2.3)) yields

$$\mathscr{F}_{,\boldsymbol{u}}[\delta\boldsymbol{u}]=\int_{t_1}^{t_2}\left\{\int_{\mathbb{R}^3}[(\nabla\cdot\boldsymbol{\Pi}-\rho_0\ddot{\boldsymbol{u}}+\rho_0\boldsymbol{f})\cdot\delta\boldsymbol{u}]\,\mathrm{d}V+\int_{\partial\Omega}[(\boldsymbol{T}-\boldsymbol{N}\cdot[\![\boldsymbol{\Pi}]\!])\cdot\delta\boldsymbol{u}]\,\mathrm{d}S\right\}\mathrm{d}t=0, \tag{2.15}$$

where $\boldsymbol{\Pi}$ is the *total first Piola–Kirchhoff* stress tensor (see [9])

$$\boldsymbol{\Pi}\equiv-\left(\frac{\partial\mathscr{E}}{\partial\boldsymbol{F}}\right)^{T}=\begin{cases}\rho_0\left(\dfrac{\partial\psi}{\partial\boldsymbol{C}}\right)\cdot\boldsymbol{F}^{T}+\dfrac{1}{\mu_0 J}\boldsymbol{B}(\boldsymbol{F}\cdot\boldsymbol{B})-\dfrac{1}{2\mu_0 J}(\boldsymbol{B}\cdot\boldsymbol{C}\cdot\boldsymbol{B})\boldsymbol{F}^{-1}; & \forall\boldsymbol{X}\in\Omega,\\[2ex] \dfrac{1}{\mu_0 J}\boldsymbol{B}(\boldsymbol{F}\cdot\boldsymbol{B})-\dfrac{1}{2\mu_0 J}(\boldsymbol{B}\cdot\boldsymbol{C}\cdot\boldsymbol{B})\boldsymbol{F}^{-1}; & \forall\boldsymbol{X}\in\mathbb{R}^3\backslash\Omega.\end{cases} \tag{2.16}$$

The arbitrariness of $\delta \boldsymbol{u}$, (2.16) yields the following differential equation and boundary/interface condition

$$\boldsymbol{\nabla}\cdot\boldsymbol{\Pi} + \rho_0 \boldsymbol{f} = \rho_0 \ddot{\boldsymbol{u}};\ \forall \boldsymbol{X} \in \mathbb{R}^3, \quad \boldsymbol{N}\cdot[\![\boldsymbol{\Pi}]\!] = \boldsymbol{T};\ \forall \boldsymbol{X} \in \partial\Omega, \tag{2.17}$$

where one recognizes the reference configuration linear momentum balance of continuum mechanics.

Eulerian version. We complete (2.9) by recording the relation between the total stress measure of the reference configuration, the first Piola–Kirchhoff stress $\boldsymbol{\Pi}$ to the Cauchy stress tensor $\boldsymbol{\sigma}$, its current configuration counterpart as well as the reference mechanical (pseudo-)traction vector $\boldsymbol{T}$ and the current mechanical traction vector $\boldsymbol{t}$

$$\boldsymbol{\Pi} = J\boldsymbol{F}^{-1}\cdot\boldsymbol{\sigma}, \quad \boldsymbol{T}\,\mathrm{d}S = \boldsymbol{t}\,\mathrm{d}s,\ (\boldsymbol{n}\,\mathrm{d}s = J\boldsymbol{N}\cdot\boldsymbol{F}^{-1}\,\mathrm{d}S). \tag{2.18}$$

Consequently, the current configuration version of the mechanical constitutive relation (2.16) gives

$$\boldsymbol{\sigma} = \begin{cases} 2\rho\boldsymbol{F}\cdot\dfrac{\partial\psi}{\partial\boldsymbol{C}}\cdot\boldsymbol{F}^T + \dfrac{1}{\mu_0}[\boldsymbol{b}\boldsymbol{b} - \dfrac{1}{2}(\boldsymbol{b}\cdot\boldsymbol{b})\boldsymbol{I}]; & \forall \boldsymbol{x} \in \omega, \\ \dfrac{1}{\mu_0}[\boldsymbol{b}\boldsymbol{b} - \dfrac{1}{2}(\boldsymbol{b}\cdot\boldsymbol{b})\boldsymbol{I}]; & \forall \boldsymbol{x} \in \mathbb{R}^3\backslash\omega. \end{cases} \tag{2.19}$$

The current configuration equilibrium equation and boundary/interface condition counterpart of (2.17) is

$$\boldsymbol{\nabla}\cdot\boldsymbol{\sigma} + \rho\boldsymbol{f} = \rho\ddot{\boldsymbol{u}};\ \forall \boldsymbol{x} \in \mathbb{R}^3 \quad \text{and} \quad \boldsymbol{n}\cdot\boldsymbol{\sigma} = \boldsymbol{t};\ \forall \boldsymbol{x} \in \partial\omega. \tag{2.20}$$

(b) Constitutive choices

For isotropic materials in three dimensions, the most general form of their specific free energy can be expressed as a function of six invariants, three purely mechanical I_1, I_2, I_3 and three magneto-mechanical J_1, J_2, J_3. Since we are interested in two dimensions problems, we only need four invariants for the free energy, namely

$$\psi(\boldsymbol{C},\boldsymbol{B}) = \psi(I_1, I_2, J_1, J_2); \quad I_1 \equiv \mathrm{tr}(\boldsymbol{C}),\ I_2 \equiv \det\boldsymbol{C} = J^2,\ J_1 \equiv \boldsymbol{B}\cdot\boldsymbol{B},\ J_2 \equiv \boldsymbol{B}\cdot\boldsymbol{C}\cdot\boldsymbol{B}. \tag{2.21}$$

The specific free energy, or equivalently the reference energy density $W(\boldsymbol{C},\boldsymbol{B})$, is decomposed into a purely mechanical part and a magneto-mechanical part (see [10]),

$$\psi(\boldsymbol{C},\boldsymbol{B}) = \psi_{\mathrm{mech}}(\boldsymbol{C}) + \psi_{\mathrm{mag}}(\boldsymbol{C},\boldsymbol{B}) \quad m \quad \rho_0\psi(\boldsymbol{C},\boldsymbol{B}) \equiv W(\boldsymbol{C},\boldsymbol{B}) = W_{\mathrm{mech}}(\boldsymbol{C}) + W_{\mathrm{mag}}(\boldsymbol{C},\boldsymbol{B}). \tag{2.22}$$

Mechanical energy density. For the mechanical reference energy density $W_{\mathrm{mech}}(\boldsymbol{C})$, a neo-Hookean behaviour is chosen,

$$W_{\mathrm{mech}}(I_1, I_2) = G\left[\frac{1}{2}(I_1 - 2 - \ln I_2) + \frac{\nu}{1-2\nu}(\sqrt{I_2} - 1)^2\right], \tag{2.23}$$

where ν denotes the three-dimensional Poisson ratio[6] ($-1 < \nu < 0.5$) and G the shear modulus. More refined choices may be relevant for modelling metals (e.g. [7]), but the neo-Hookean model is perfectly adequate here, given the small strains expected (see [11]).

Magnetic energy density. The magnetization law for ferromagnetic conductors is an old and well-researched topic that depends on many external factors: dissipation (e.g. [14]), anisotropy (e.g. [15]), residual stresses (e.g. [16]), multi axial loading (e.g. [17]), rate and inertia effects (e.g. [18]), to name but a few. Given that the magnetization response of the conductor is not the primary focus of this study, we use a simple model proposed in [19].

The magnetic reference energy density W_{mag} used subsequently in the calculations assumes an non-hysteretic magnetic behaviour (no dissipative phenomena considered). For small strains and an isotropic energy density W_{mag} depends, at first approximation, solely on the magnitude

[6]A more appropriate expression should involve the two-dimensional Poisson ratio $\nu' \equiv \nu/(1-\nu)$ in which case the coefficient of the volumetric part should read $\nu'/(1-\nu')$.

of the magnetic field. An appropriate choice (see [11]) is $W_{\text{mag}}(\boldsymbol{C},\boldsymbol{B}) = W_{\text{mag}}(I_2, J_2) = W_{\text{mag}}(||\boldsymbol{b}||)$, since from (2.9) $\boldsymbol{b}\cdot\boldsymbol{b} = ||\boldsymbol{b}||^2 = J_2/I_2$.

For small magnetic fields, the model must capture the linear magnetization behaviour of the material, i.e. predict its initial magnetic susceptibility χ_0.[7] The model should also account for saturation, i.e. asymptotically approach the saturation magnetization m_s at large h-field vectors. To this effect, the following simple saturation magnetization law is used (see [19])

$$W_{\text{mag}}(||\boldsymbol{b}||) = \frac{\mu_0 m_s^2}{\chi_0} \ln\left[\cosh\left(\frac{\chi_0||\boldsymbol{b}||}{\mu_0 m_s}\right)\right]. \tag{2.24}$$

For small strains, i.e. when $||\boldsymbol{\epsilon}|| \ll 1$, where $\boldsymbol{\epsilon} \equiv (1/2)(\nabla\boldsymbol{u} + \boldsymbol{u}\nabla)$, but arbitrary magnetic field vector amplitudes $||\boldsymbol{b}||$ and recalling that $\boldsymbol{C} = \boldsymbol{I} + 2\boldsymbol{\epsilon} + O||\boldsymbol{\epsilon}||^2$, the expressions for the magnetization $\boldsymbol{m}$ and the total stress $\boldsymbol{\sigma}$ simplify considerably. It has been shown in [10], using asymptotic expansions in (2.13), (2.19) and (2.21), that for the energy densities adopted in (2.22), (2.23) and (2.24), the total stress $\boldsymbol{\sigma}$ can be approximated by the sum of a purely elastic part $\overset{e}{\boldsymbol{\sigma}}(\boldsymbol{\epsilon})$ and a purely magnetic part $\overset{m}{\boldsymbol{\sigma}}(\boldsymbol{b})$

$$\left.\begin{aligned}
&\boldsymbol{m} = \begin{cases} -\dfrac{\partial W_{\text{mag}}(||\boldsymbol{b}||)}{\partial \boldsymbol{b}} = \dfrac{\chi(||\boldsymbol{b}||)}{\mu_0[1+\chi(||\boldsymbol{b}||)]}\boldsymbol{b}; & \forall\, \boldsymbol{x} \in \omega, \\ \boldsymbol{0}; & \forall\, \boldsymbol{x} \in \mathbb{R}^3\backslash\omega, \end{cases} \\
&\boldsymbol{\sigma} = \overset{e}{\boldsymbol{\sigma}} + \overset{m}{\boldsymbol{\sigma}}; \qquad \forall\, \boldsymbol{x} \in \mathbb{R}^3 \\
&\overset{e}{\boldsymbol{\sigma}} = \begin{cases} \lambda \text{tr}(\boldsymbol{\epsilon})\boldsymbol{I} + 2G\boldsymbol{\epsilon}; & \forall\, \boldsymbol{x} \in \omega, \\ \boldsymbol{0}; & \forall\, \boldsymbol{x} \in \mathbb{R}^3\backslash\omega. \end{cases} \\
\text{and} \quad &\overset{m}{\boldsymbol{\sigma}} = \begin{cases} \dfrac{1}{\mu_0}[\boldsymbol{bb} - \dfrac{1}{2}(\boldsymbol{b}\cdot\boldsymbol{b})\boldsymbol{I}] - \dfrac{\chi(||\boldsymbol{b}||)}{\mu_0[1+\chi(||\boldsymbol{b}||)]}[\boldsymbol{bb} - (\boldsymbol{b}\cdot\boldsymbol{b})\boldsymbol{I}]; & \forall\, \boldsymbol{x} \in \omega, \\ \dfrac{1}{\mu_0}[\boldsymbol{bb} - \dfrac{1}{2}(\boldsymbol{b}\cdot\boldsymbol{b})\boldsymbol{I}]; & \forall\, \boldsymbol{x} \in \mathbb{R}^3\backslash\omega, \end{cases}
\end{aligned}\right\} \tag{2.25}$$

where $\chi(||\boldsymbol{b}||)$ is the material's '*magnetic susceptibility*'[8] since $\boldsymbol{m} = \chi(||\boldsymbol{b}||)\boldsymbol{h}$. The initial magnetic susceptibility introduced in (2.24) is $\chi_0 = \chi(0)$.

Based on (2.24), one obtains from (2.25) the following magnetization as a function of the applied h-field vector, depicted in figure 2 in dimensionless form where the reference magnetization has the saturation value $m_{\text{ref}} = m_s$ and the reference h-field vector is taken to be $h_{\text{ref}} = m_s/\chi_0$. It is also useful to establish a range where the linear magnetic response is a reasonable approximation; to this effect, we set $h_l = 0.6 \times 10^{-2} h_{\text{ref}}$ as the limit for the linear range for the magnetic response $0 \le h \le h_l$, as seen in figure 2*a*.

As seen from (2.25) for small strains, the determination of the magnetic stresses $\overset{m}{\boldsymbol{\sigma}}$ depends solely on the magnetic field vector $\boldsymbol{b}$, which in turn requires only finding the magnetic vector potential $\boldsymbol{a}$ by solving the Eulerian version of the magnetics equations (2.10) to (2.13) in conjunction with (2.24) and $(2.25)_1$. The determination of the elastic stresses $\overset{e}{\boldsymbol{\sigma}}$ in $(2.25)_3$ requires the determination of the displacement $\boldsymbol{u}$, which can be found by solving the Eulerian version of the mechanics equations (2.20) in conjunction with (2.25). Since only the total forces exerted on the conductors are of interest, the determination of the displacement field is not necessary, as will be discussed in §2d.

[7]It has been shown in [10] that for small strains and magnetic fields the magnetic response is consistently characterized by two constants: magnetic susceptibility χ—considered here—and magnetostriction Λ—set to zero by selection of the energy density in (2.24).

[8]We note here that for a more general magnetic energy density W_{mag} the linearization procedure would have added an additional term to $\overset{m}{\boldsymbol{\sigma}}$ in (2.25) $\Lambda(||\boldsymbol{b}||)/[\mu_0(1+\chi(||\boldsymbol{b}||))]\boldsymbol{bb}$, where $\Lambda(||\boldsymbol{b}||)$ a *magneto mechanical coupling* coefficient which gives the curvature of the strain versus magnetic field in a stress-free uniaxial magnetostriction experiment.

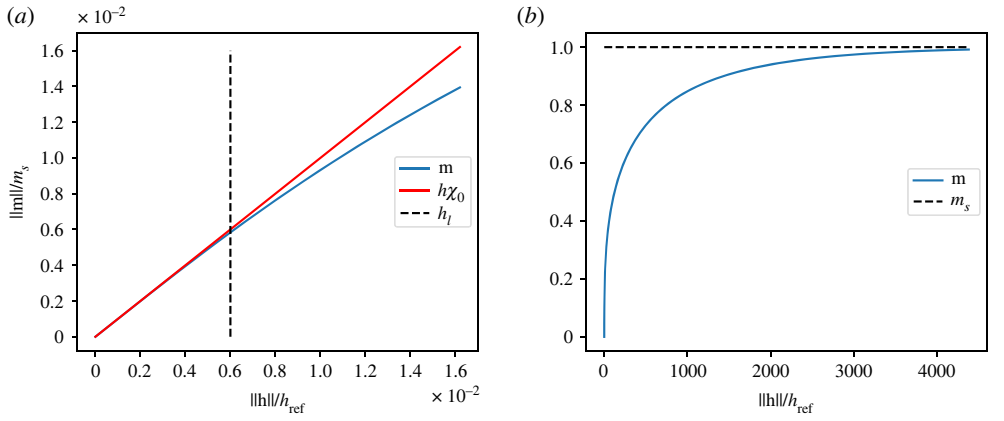

Figure 2. Nonlinear magnetization law in dimensionless form: magnetization as a function of applied h-field vector. (*a*) Low h-field vector response: $0 \leq h/h_{\text{ref}} \leq 1.6 \times 10^{-2}$. (*b*) Full h-field vector response: $0 \leq h/h_{\text{ref}} \leq 5 \times 10^{3}$.

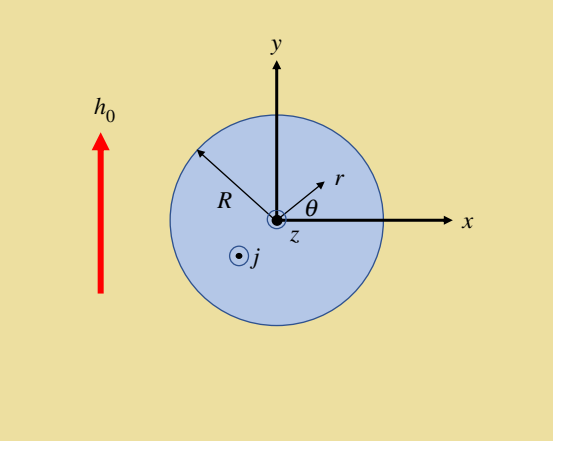

Figure 3. Cross section of a cylindrical conductor of radius R subjected to a current of uniform density $\boldsymbol{j} = j\boldsymbol{e}_z$ and a remote h-field vector of magnitude $\boldsymbol{h}_0 = h_0\boldsymbol{e}_y$.

(c) Analytical solution for a single conductor with linear magnetic response

Assume a circular section conductor of radius R subjected to a current of uniform density j along the cylinder's axis ($\boldsymbol{j} = j\boldsymbol{e}_z$) and a remote h-field vector of magnitude h_0 along the y direction ($\boldsymbol{h}_0 = h_0\boldsymbol{e}_y$) as shown in figure 3. Of interest are the resulting h-field vector $\boldsymbol{h}$, magnetization $\boldsymbol{m}$ and magnetic stress $\overset{m}{\boldsymbol{\sigma}}$, which for the case of a linear magnetic constitutive law can be calculated analytically.

By superposing the solutions for the remote h-field vector h_0 and the uniform current density j, one can verify that the solution of Ampère's equation in (2.11) is

$$r > R: \begin{cases} h_x = \left(\frac{R}{r}\right)^2 [(h_0 - h_{in})\sin(2\theta) - \frac{jr}{2}\sin\theta], \\ h_y = h_0 + \left(\frac{R}{r}\right)^2 \left[(h_{in} - h_0)\cos(2\theta) + \frac{jr}{2}\cos\theta\right], \end{cases} \quad 0 \leq r \leq R: \begin{cases} h_x = -\frac{jr}{2}\sin\theta, \\ h_y = h_{in} + \frac{jr}{2}\cos\theta. \end{cases} \tag{2.26}$$

For the case of a linear, isotropic magnetic response, i.e. $\boldsymbol{m} = \chi_0\boldsymbol{h}$ and recalling that inside the conductor $\boldsymbol{b} = \mu_0(\boldsymbol{h} + \boldsymbol{m})$ and outside $\boldsymbol{b} = \mu_0\boldsymbol{h}$ one obtains by using the boundary condition for

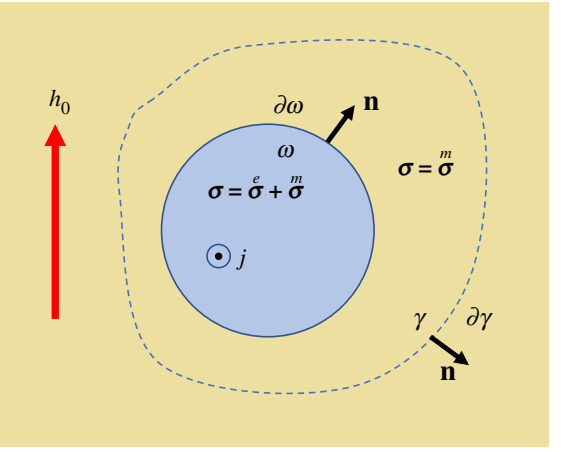

Figure 4. Calculating the Lorentz forces $\boldsymbol{F}_L$ on a conductor subjected to a current of density j and a remote h-field vector of magnitude h_0 using contour integrals.

the magnetic field vector $\boldsymbol{b}$

$$h_{\text{in}} = \frac{2(1+\chi_0)}{2+\chi_0} h_0; \quad 0 \le r \le R: \begin{cases} m_x = -\chi_0 \dfrac{jr}{2} \sin\theta, \\ m_y = \chi_0 \left[\dfrac{2}{2+\chi_0} h_0 + \dfrac{jr}{2} \cos\theta \right]. \end{cases} \tag{2.27}$$

From (2.26) and (2.27), the magnetic field vector $\boldsymbol{b}$ is thus found to be

$$r > R: \begin{cases} b_x = \mu_0 \left(\dfrac{R}{r}\right)^2 \left[\dfrac{\chi_0}{2+\chi_0} h_0 \sin(2\theta) - \dfrac{jr}{2} \sin\theta \right], \\ b_y = \mu_0 \left\{ h_0 - \left(\dfrac{R}{r}\right)^2 \left[\dfrac{\chi_0}{2+\chi_0} h_0 \cos(2\theta) - \dfrac{jr}{2} \cos\theta \right] \right\}, \end{cases}$$

and

$$0 \le r \le R: \begin{cases} b_x = -\mu_0(1+\chi_0) \dfrac{jr}{2} \sin\theta, \\ b_y = \mu_0(1+\chi_0) \left[\dfrac{2}{2+\chi_0} h_0 + \dfrac{jr}{2} \cos\theta \right]. \end{cases} \tag{2.28}$$

The above solution is valid as long as the linear magnetic constitutive response is a reasonable approximation, i.e. $||\boldsymbol{b}||_{\max} \le b_l$, where $b_l = \mu_0 h_l$ (figure 2*a*). A straightforward calculation of the magnetic field vector norm $||\boldsymbol{b}|| = (b_x^2 + b_y^2)^{1/2}$ gives from (2.28) that the maximum occurs at the boundary $(r, \theta) = (R, 0)$

$$||\boldsymbol{b}||_{\max} = \mu_0(1+\chi_0) \left[\frac{2}{2+\chi_0} h_0 + \frac{jR}{2} \right] = b_l, \tag{2.29}$$

thus establishing the maximum value combination of the remote h-field vector and current density for a near-linear magnetic response.

Having obtained the magnetic field vector $\boldsymbol{b}$ inside and outside the conductor, we can calculate the magnetic stress $\overset{m}{\boldsymbol{\sigma}}$, both inside and outside the conductor from (2.25).

(d) Calculating forces on conductors using contour integrals

Single conductor. We start by defining the total force per unit length $\boldsymbol{F}_L$ on a conductor occupying domain ω with boundary $\partial\omega$ subjected to a current of density j and a remote h-field vector $\boldsymbol{h}_0$ as shown in figure 4.

Since the traction exerted by the magnetic field on the conductor is $\boldsymbol{n}\cdot\boldsymbol{\sigma}$ the force is

$$\boldsymbol{F}_L \equiv \int_{\partial\omega} \mathbf{n}\cdot\boldsymbol{\sigma}\, \mathrm{d}l. \tag{2.30}$$

Using Gauss' divergence theorem in the domain $\gamma\setminus\omega$ and recalling that the total stress there is the magnetic stress (i.e. $\boldsymbol{\sigma} = \overset{m}{\boldsymbol{\sigma}}$) and recalling the equilibrium equation (2.20) for that domain $\nabla\cdot\overset{m}{\boldsymbol{\sigma}} = \mathbf{0}$ since the material density in vacuum (the domain $\gamma\setminus\omega$) is $\rho = 0$

$$\int_{\partial(\gamma\setminus\omega)} \mathbf{n}\cdot\boldsymbol{\sigma}\, \mathrm{d}l = \int_{\gamma\setminus\omega} \nabla\cdot\boldsymbol{\sigma}\, \mathrm{d}s = \int_{\gamma\setminus\omega} \nabla\cdot\overset{m}{\boldsymbol{\sigma}}\, \mathrm{d}s = 0 \quad\Longrightarrow \int_{\partial\gamma} \mathbf{n}\cdot\boldsymbol{\sigma}\, \mathrm{d}l = \int_{\partial\omega} \mathbf{n}\cdot\boldsymbol{\sigma}\, \mathrm{d}l = \boldsymbol{F}_L, \tag{2.31}$$

where γ is an arbitrary domain completely surrounding ω, i.e. $\gamma \supset \omega$ as seen in figure 4.

Taking the contour $\partial\gamma$ as far as possible from $\partial\omega$, one can consider a circle of radius $r \gg R$ in which case the dominant terms in the remote h-field vector $\boldsymbol{h}^\infty$ and the remote total stress $\boldsymbol{\sigma}^\infty$ yield[9] from $(2.26)_1$ and (2.25), respectively, the following expressions

$$\boldsymbol{h}^\infty = -\frac{I\sin\theta}{2\pi r}\boldsymbol{e}_x + \left[h_0 + \frac{I\cos\theta}{2\pi r}\right]\boldsymbol{e}_y \quad \text{and} \quad \boldsymbol{\sigma}^\infty = \mu_0\left[\boldsymbol{h}^\infty\boldsymbol{h}^\infty - \frac{1}{2}(\boldsymbol{h}^\infty\cdot\boldsymbol{h}^\infty)\boldsymbol{I}\right]. \tag{2.32}$$

From (2.30), the force/length $\boldsymbol{F}_L$ exerted on the conductor, comes with no surprise to be the textbook result of electromagnetics for the force on a conductor carrying a current I and subjected to a remote magnetic field vector of strength b_0 normal to the conductor

$$\boldsymbol{F}_L = \int_{\partial\gamma} \mathbf{n}\cdot\boldsymbol{\sigma}^\infty\, \mathrm{d}l = \mu_0\int_0^{2\pi}(\boldsymbol{e}_x\cos\theta + \boldsymbol{e}_y\sin\theta)\cdot\left[\boldsymbol{h}^\infty\boldsymbol{h}^\infty - \frac{1}{2}(\boldsymbol{h}^\infty\cdot\boldsymbol{h}^\infty)\boldsymbol{I}\right] r\mathrm{d}r\mathrm{d}\theta = -b_0 I\boldsymbol{e}_x. \tag{2.33}$$

It is important to note that the above result is independent of the cross section of the conductor as well as of its magnetic properties, since the method of calculating the Lorentz force $\boldsymbol{F}_L$ is based on the Maxwell stresses $\boldsymbol{\sigma}^\infty$ generated by the remote magnetic field vector $\boldsymbol{b}_0$ and the current I.

Two parallel conductors. The Lorentz force on each of the two conductors of radius R separated by a distance D is calculated from the contour integrals on the two corresponding domains $\gamma_1 \supset \omega_1$ and $\gamma_2 \supset \omega_2$ as shown in figure 5. Each domain consists of half a disc of radius $r > D$ and $\gamma_1 \cap \gamma_2$ is the $[-r, r]$ interval of the y-axis.

The h-field vector for $r \gg D$ in the case of currents of same $\boldsymbol{h}_S^\infty$ or opposite $\boldsymbol{h}_O^\infty$ direction, is given by

$$\boldsymbol{h}_S^\infty = -\frac{2I\sin\theta}{2\pi r}\boldsymbol{e}_x + \left[h_0 + \frac{2I\cos\theta}{2\pi r}\right]\boldsymbol{e}_y, \quad \boldsymbol{h}_O^\infty = h_0\boldsymbol{e}_y, \tag{2.34}$$

since in the first case (same direction currents designated by S) the influence of the electric currents on the magnetic field is additive and in the latter case (opposite direction currents designated by O) they cancel each other. The Maxwell stress $\boldsymbol{\sigma}^\infty$ at $r \gg D$ is given in terms of $\boldsymbol{h}^\infty$ by (2.32).

Calculating the contour integrals on $\partial\gamma_1$ and $\partial\gamma_2$ in clockwise direction[10], we obtain for the corresponding Lorentz forces $\boldsymbol{F}_L^{1,2}$

$$\boldsymbol{F}_{L,S}^{1,2} = \left[-b_0 I \pm \frac{1}{2\mu_0}\int_{-\infty}^{+\infty}[b_x^2(0,y) - b_y^2(0,y) + b_0^2]\mathrm{d}y\right]\boldsymbol{e}_x$$

and

$$\boldsymbol{F}_{L,O}^{1,2} = \left[\pm\frac{1}{2\mu_0}\int_{-\infty}^{+\infty}[b_x^2(0,y) - b_y^2(0,y) + b_0^2]\mathrm{d}y\right]\boldsymbol{e}_x. \tag{2.35}$$

Unlike the single conductor, we expect for the two conductors that their magnetic properties will influence the Lorentz forces due to the change of the magnetic field vector $\boldsymbol{b}$ along the y-axis, as seen from (2.35).

Infinite array of parallel conductors. We consider next an infinite array of parallel cylindrical conductors of radius R equally spaced from each other at a distance D and subjected to a remote

[9]The magnetic field for $r \gg R$ is independent of the magnetic properties of the conductor and depends solely on the total current $I = \pi R^2$, thus justifying using the linear result in (2.26) to find the dominant terms.

[10]Due to symmetry considerations one can show that the $\boldsymbol{e}_x$ component of the Lorentz forces is zero.

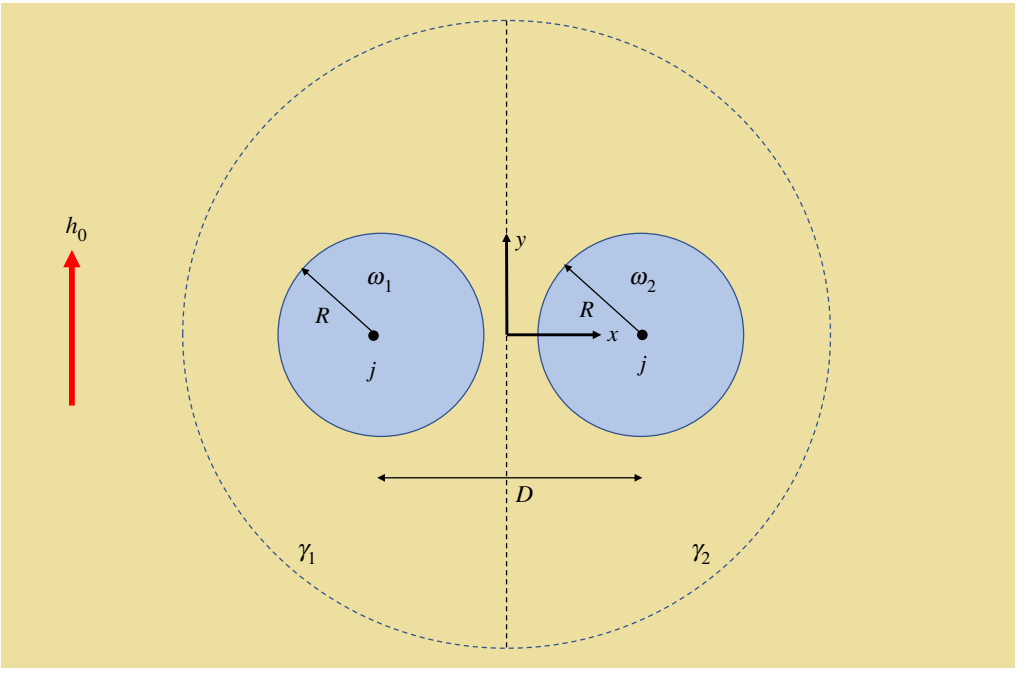

Figure 5. Calculating the Lorentz forces on two parallel conductors subjected to same or opposite direction currents of density j and a remote h-field vector of magnitude h_0 using contour integrals.

h-field vector $\boldsymbol{h}_0$ as shown in figure 6. The conductors are subjected to uniform current densities $\boldsymbol{j}$, either all in the same direction or in alternating opposite directions.

An immediate result of periodicity is that for $D \gg R$ the Lorentz force in each conductor is $F_L = \pm b_0 I \boldsymbol{e}_x$ (where the current $I = j\pi R^2$ and the $\pm$ sign depends on the current direction of the conductor at hand) since the magnetic field contribution at the centre of any given conductor due to a conductor at distance $+nD$ is cancelled by its counterpart at distance $-nD$, where $n \in \mathbb{N}$, thus leaving the magnetic field there equal to the remote magnetic field $\boldsymbol{b}_0$.

A more refined result is obtained in the case of the periodic array with same direction currents. The Lorentz force on each conductor can be calculated from the contour integral along $AB\Gamma\Delta$ as seen in figure 6,

$$F_L = \int_A^B [-\mathbf{e}_y \cdot \boldsymbol{\sigma}^\infty]\,\mathrm{d}x + \int_B^\Gamma [\mathbf{e}_x \cdot \boldsymbol{\sigma}]\,\mathrm{d}y + \int_\Gamma^\Delta [\mathbf{e}_y \cdot \boldsymbol{\sigma}^\infty]\,\mathrm{d}x + \int_\Delta^A [-\mathbf{e}_x \cdot \boldsymbol{\sigma}]\,\mathrm{d}y. \tag{2.36}$$

From periodicity, the stress $\boldsymbol{\sigma}$ is the same on the $B\Gamma$ and $A\Delta$ segments of the contour but given the opposite direction of the normal there ($\boldsymbol{n} = \pm\mathbf{e}_x$) the sum of these two integrals vanishes. For the h-field vector[11] on segments AB and $\Gamma\Delta$ as well as the stress there (recall (2.32)), we have

$$\boldsymbol{h}^\infty = \pm\frac{I}{2}\mathbf{e}_x + h_0\mathbf{e}_y \quad \text{and} \quad \boldsymbol{\sigma}^\infty = \mu_0\left[\boldsymbol{h}^\infty\boldsymbol{h}^\infty - \frac{1}{2}(\boldsymbol{h}^\infty \cdot \boldsymbol{h}^\infty)\boldsymbol{I}\right], \tag{2.37}$$

and hence the non-trivial contribution from these segments to the Lorentz force gives $\boldsymbol{F}_L = \pm b_0 I \mathbf{e}_x$ depending on the direction of the current I. It is interesting to note that the Lorentz force in an infinite, periodic array of conductors, all with currents in the same direction, is independent of the conductors' magnetic properties, irrespectively of how close they are!

For the case of currents with alternating directions, a similar argument on the contour $AB\Gamma'\Delta'$ will give a zero total Lorentz force $\boldsymbol{F}_L = \boldsymbol{F}_L^1 + \boldsymbol{F}_L^2 = 0$ since $\boldsymbol{h}^\infty = h_0\mathbf{e}_y$, where the superscripts refer

[11] The $\pm$ sign corresponds to each different x-segment of the contour.

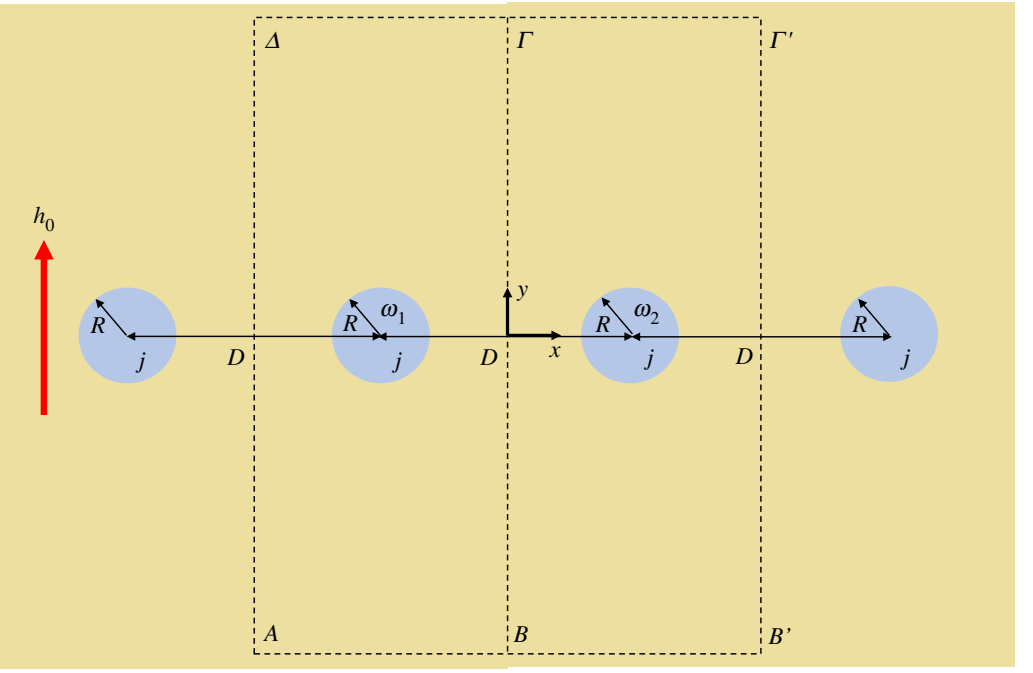

Figure 6. Calculating the Lorentz forces on parallel conductors subjected to same or alternating direction currents of density j and a remote h-field vector of magnitude h_0 in an infinite array using contour integrals.

to the *left* and *right* conductors in the $AB\Gamma'\Delta'$ contour. As previously discussed for $D \gg R$, $\boldsymbol{F}_L^1 = -\boldsymbol{F}_L^2 = \pm b_0 l \boldsymbol{e}_x$, but for closer spacing of the conductors, their magnetic properties will influence their Lorentz force.

3. Numerical (FEM) implementation

We apply here the general theory developed in §2a,b to the boundary value problem of the ferromagnetic conductors subjected to a remote magnetic field and an electric current. The numerical solution is based on an FEM discretization of a two dimensions, quasi-static problem and solved by extremization of a simplified version of the Lagrangian (2.2) based on the energy density adopted in §2b. Due to the small strains involved and the simplified expression for the total stress in (2.25), only the magnetic field vector **b**—and hence the magnetic vector potential a—needs to be calculated in order to determine the magnetic stress $\overset{m}{\boldsymbol{\sigma}}$ which is the basis for calculating the total force applied in each semiconductor, as discussed in §2d. Had one been interested in calculating also the elastic stress $\overset{e}{\boldsymbol{\sigma}}$, the fully coupled problem would have to be solved to also determine the displacement field $\boldsymbol{u}$ (see [11]).

Solution method is based on a two-dimensional model (plane strain assumed, see figure 1), where all field quantities are assumed independent of z. It involves no external body forces, no mechanical tractions or current sheets and has negligible induced currents and acceleration terms, thus requiring only a spatial discretization of the corresponding quasi-static problem. Moreover, since we are not interested in calculating the displacement field $\boldsymbol{u}$, the current configuration (Eulerian) formulation of the problem is adopted with all field quantities functions of the current position vector $\boldsymbol{x}$.

The Lagrangian of the system defined in (2.2) (kinetic minus potential energy: $\mathscr{L} = \mathscr{K} - \mathscr{P}$), in the absence of the kinetic energy ($\mathscr{K} = 0$) equals minus the potential energy ($\mathscr{L} = -\mathscr{P}$), which for

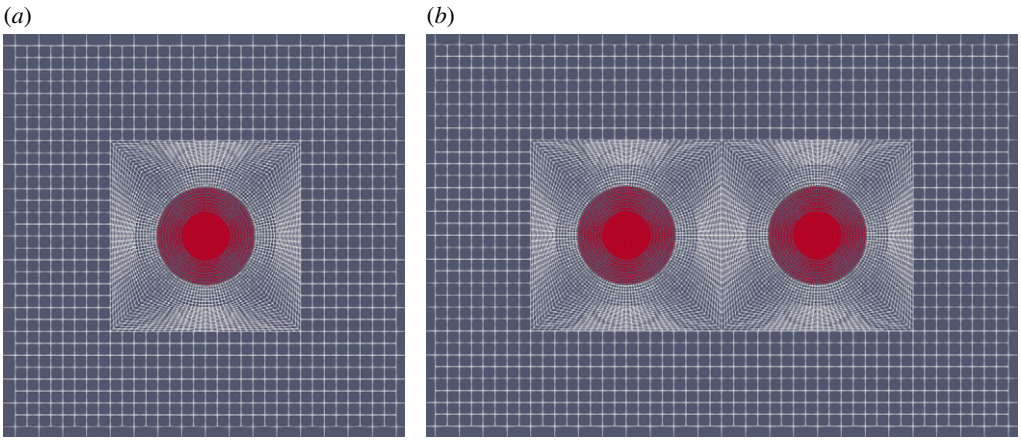

Figure 7. Typical FEM meshes used for calculating the magnetic vector potential a inside and outside the conductor domain. In (*a*), for a single conductor of radius R and in (*b*) for two conductors of same radius R at a distance $D = 4R$. (*a*) Mesh for the magnetic vector potential a in ω and $\mathbb{R}\backslash\omega$, (*b*) mesh for the magnetic vector potential a in $\omega_1 \cup \omega_2$ and $\mathbb{R}\backslash(\omega_1 \cup \omega_2)$.

the case of no external body forces, no mechanical surface tractions or current sheets becomes

$$\mathscr{P} = \int_{\mathbb{R}^2} W(||\boldsymbol{b}||)\,\mathrm{d}s - \int_{\omega} (\boldsymbol{j}\cdot\boldsymbol{a})\,\mathrm{d}s \quad \text{and} \quad W(||\boldsymbol{b}||) \equiv W_{\mathrm{mag}}(||\boldsymbol{b}||) + \frac{1}{2\mu_0}||\boldsymbol{b}||^2,\ \boldsymbol{b} = \nabla \times a, \tag{3.1}$$

where $W(||\boldsymbol{b}||)$ is the system's total energy density. The conductor's magnetic energy density is only defined in the domain ω, i.e. $W_{\mathrm{mag}}(||\boldsymbol{b}(\boldsymbol{x})||) \neq 0;\ \forall\, \boldsymbol{x} \in \omega$ and $W_{\mathrm{mag}}(||\boldsymbol{b}(\boldsymbol{x})||) = 0;\ \forall\, \boldsymbol{x} \in \mathbb{R}^2\backslash\omega$.

Since a plane strain boundary value problem is considered, integration over the entire domain involves $\mathbb{R}^2$ and the cross section of the stator domain has boundary $\partial\omega$. Moreover, the in-plane magnetic field vector ($\boldsymbol{b} = \nabla \times \boldsymbol{a}$, see (2.12)) is derived from the magnetic vector potential $\boldsymbol{a} = a(x, y)\boldsymbol{e}_z$, requiring only one scalar field variable for its determination, i.e. $\boldsymbol{b} = a_{,y}\boldsymbol{e}_x - a_{,x}\boldsymbol{e}_y$. Consequently, the Coulomb gauge condition $\nabla \cdot \boldsymbol{a}$ (see footnote 3) is automatically satisfied. As a result of Ampère's Law (2.11) and the in-plane h-field vector, the externally applied currents can only be of the form $\boldsymbol{j} = j_z(x, y)\boldsymbol{e}_z$, thus automatically satisfying charge conservation $\nabla \cdot \boldsymbol{j} = 0$. Thus, the solution of the magnetic boundary value problem, based on the FEM discretization of (3.1), requires only one scalar field variable $a(x, y)$[12].

For the sake of simplicity and meshing flexibility, the elements chosen for the FEM spatial discretization are quadrilateral two-dimensional elements with a second-order polynomial interpolation and nine nodes, using a 3×3 Gauss numerical integration scheme. The corresponding UEL (user element) is provided to *DealII* in the final assembly of the global force vector and stiffness matrix of the problem. The accuracy of the numerical code is verified using the analytical solution for the single conductor with a linear magnetization law presented in §2c. The boundary condition imposed on the computational domain is $\widehat{a}(x, y) = 0$. To ensure that this assumption does not affect the accuracy of the results, we use rectangular domains of minimum dimensions $120R \times 120R$, so that their boundaries are at least $60R$ away from the centre of each conductor. Numerical simulations typically require 50 000 d.o.f. meshes. Only the central section of the much larger computational domain is shown in figure 7, to better depict the denser mesh inside and near the conductors.

[12]For added simplicity, the numerical code is based on the discretization of the perturbation field $\widehat{a}(x, y) \equiv a(x, y) - a_0(x, y)$ resulting from the presence of the conductor; in its absence $a(x, y) = a_0(x, y) = -xb_0$.

4. Results

We start with a remark about the validity of the uniform current assumption that is typically adopted in the electrical engineering literature and hence in the ensuing numerical calculations. In order to satisfy the Maxwell–Gauss equations pertaining to the electric field resulting inside the conductor due to the electric current (in addition to the Maxwell–Ampère equations presented in §2), we make the simplifying assumption of a negligible conductor resistivity, resulting in a negligible electric field inside (and hence outside of) the conductor. In a simulation that accounts for ohmic dissipation in the conductor Hall effects [20] will have to be considered, resulting in non-uniform current densities inside a conductor.

In presenting the results, we adopt a dimensionless form and hence, we define the following reference quantities based on the conductor's material properties and geometry, i.e. its radius R

$$m_{\text{ref}} = m_s, \quad b_{\text{ref}} = m_s \mu_0, \quad h_{\text{ref}} = \frac{m_s}{\chi_0}, \quad j_{\text{ref}} = \frac{h_{\text{ref}}}{R} = \frac{m_s}{R\chi_0}, \quad F_{\text{ref}} = b_{\text{ref}} j_{\text{ref}} \pi R^2 = \frac{m_s^2 \mu_0 \pi R}{\chi_0}. \tag{4.1}$$

We have in mind a typical ferromagnetic wire of radius 1.5 mm as the base case and hence all subsequent numerical calculations presented here use the values: $R = 1.5 \times 10^{-3}$ m, $\chi_0 = 2.5 \times 10^3$, $m_s = 1.7 \times 10^6$ A m^{-1} and $\mu_0 = 4\pi \times 10^{-7}$ N A^{-2}. The reference values in the *MKSA* system of units are: $h_{\text{ref}} = 0.68$ A m^{-1}, $j_{\text{ref}} = 0.45 \times 10^6$ A m^{-2} and $b_{\text{ref}} = 2.14$ T.

A remark about the range of magnetic fields and electric currents used in the ensuing calculations is in order. As the most upscale laboratory magnets generate magnetic fields of the order of 1 T to 2 T, we investigate magnetic fields up to 0.7 b_{ref}. To avoid excessive ohmic heating of the conductors and by assuming (to be on the conservative side) adiabatic heating, the current density is related to the temperature increase rate $\dot{\theta}$ (in $^\circ$K s^{-1}) by

$$j = (\gamma \rho_0 c_p \dot{\theta})^{1/2} \approx 3.13 \times 10^6 (\dot{\theta})^{1/2} \,\text{A m}^{-2}, \tag{4.2}$$

where γ is the electric conductivity, c_p is the specific heat and ρ_0 is the mass density of the conductor and where we have also assumed typical values for a ferromagnetic material. We present calculations here for current densities up to 6.36 j_{ref}, which correspond to a temperature increase rate of about 0.83°K s^{-1}.

(a) Single conductor under magnetic field and electric current

We start by presenting in figure 8 the magnetic field for a single conductor with a circular section of radius R, subjected to a uniform current density $\boldsymbol{j} = j\boldsymbol{e}_z$ and a remote external magnetic field vector $\boldsymbol{b}_0 = b_0 \boldsymbol{e}_y$ (see geometry in figure 3). More specifically, contours of the dimensionless magnetization field norm $||\boldsymbol{m}||/m_s$ are depicted in figure 8*a* for near-linear magnetic response (low values of external magnetic field vector and current, respectively $b_0 = 0.52 \times 10^{-4}\ b_{\text{ref}}$ and $j = 2 \times 10^{-4}\ j_{\text{ref}}$) and in figure 8*b* for near saturation magnetic response (high values of external magnetic field vector and current, respectively $b_0 = 0.66\ b_{\text{ref}}$ and $j = 5.25\ j_{\text{ref}}$).

For a rigid, isotropic ferromagnetic material of circular section in two dimensions or spherical shape in three-dimensional subjected to an external magnetic field it is known (e.g. [21]) that the h-field vector and hence the magnetization inside the conductor is uniform, independently of the magnetic constitutive law. It is the presence of the magnetic field gradient due to the applied current that introduces a gradient of the magnetization field inside the conductor, as seen for the special case of a linear magnetic response from (2.27).

For the near-linear magnetic regime, we observe in figure 8*a* that the magnetization is minimized (near zero) at the left side, since the external and current-induced magnetic fields are in opposite directions in that location, and maximized on the right side when these same fields act in the same direction, as expected from (2.27). For the near saturation response, we observe from figure 8*b* that the entire domain has a nearly uniform magnetization (of about $0.82 m_s$) and the influence of the current on the magnetization is almost negligible. Numerical simulations with

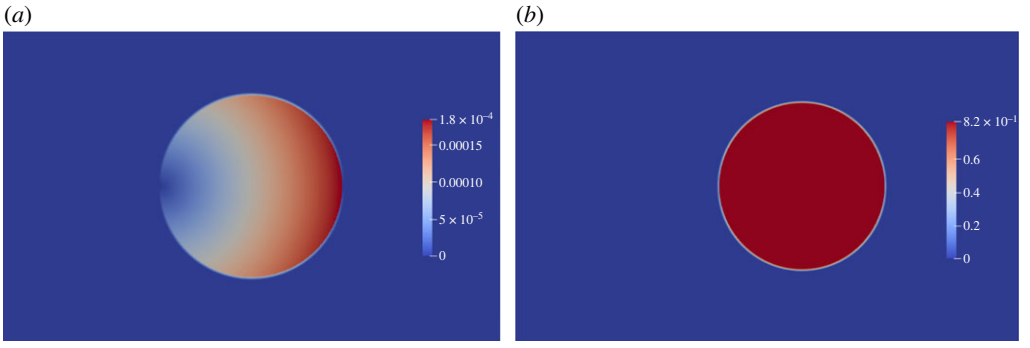

Figure 8. Contours of the magnetization vector field norm $||\boldsymbol{m}||/m_s$ for a conductor subjected to an electric current and a remote magnetic field. In (*a*), for low remote magnetic field vector $b_0 = 0.52 \times 10^{-4}\, b_{\text{ref}}$ and current $j = 2 \times 10^{-4}\, j_{\text{ref}}$ where the entire section is in the near-linear regime of magnetization. In (*b*), for high remote magnetic field vector $b_0 = 0.66\, b_{\text{ref}}$ and current $j = 5.25\, j_{\text{ref}}$, where the entire conductor is near the saturation regime of magnetization. (*a*) $||\boldsymbol{m}||/m_s$ Near linear magnetic response, (*b*) $||\boldsymbol{m}||/m_s$ Near saturation magnetic response.

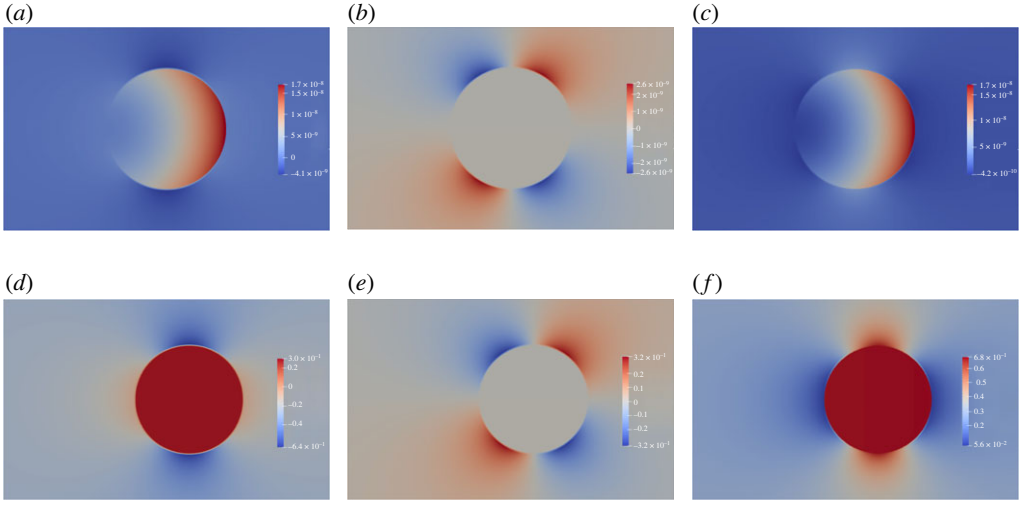

Figure 9. Contours for the dimensionless magnetic stress $\overset{m}{\boldsymbol{\sigma}}/\mu_0 m_s^2$ components for a conductor subjected to an electric current and a remote magnetic field. In (*a*), (*b*) and (*c*), for low remote magnetic field vector $b_0 = 0.52 \times 10^{-4}\, b_{\text{ref}}$ and current $j = 2 \times 10^{-4}\, j_{\text{ref}}$ where the entire section is in the near-linear regime of magnetization. In (*d*), (*e*) and (*f*), for high remote magnetic field vector $b_0 = 0.66\, b_{\text{ref}}$ and current $j = 5.25\, j_{\text{ref}}$, where the entire conductor is near the saturation regime of magnetization. (*a*) $\overset{m}{\sigma}_{xx}/\mu_0 m_s^2$ Near linear response, (*b*) $\overset{m}{\sigma}_{xy}/\mu_0 m_s^2$ Near linear response, (*c*) $\overset{m}{\sigma}_{yy}/\mu_0 m_s^2$ Near linear response, (*d*) $\overset{m}{\sigma}_{xx}/\mu_0 m_s^2$ Near saturation response, (*e*) $\overset{m}{\sigma}_{xy}/\mu_0 m_s^2$ Near saturation response and (*f*) $\overset{m}{\sigma}_{yy}/\mu_0 m_s^2$ Near saturation response.

much higher currents $j \approx 10^2\, j_{\text{ref}}$ (not reported here) produce non-uniform magnetization fields with a strong gradient that increases with an increasing current.

Next, we present the magnetic stress field components in figure 9 for the same single conductor. More specifically, contours of the dimensionless magnetic stress field $\overset{m}{\boldsymbol{\sigma}}/\mu_0 m_s^2$ components are depicted in figure 9*a–c*, for near-linear magnetic response (low values of external and current-induced *h*-field vectors, same as in figure 8*a*) and in figure 9*d–f* for near saturation magnetic response (high values of external and current-induced *h*-field vectors, same as in figure 8*b*).

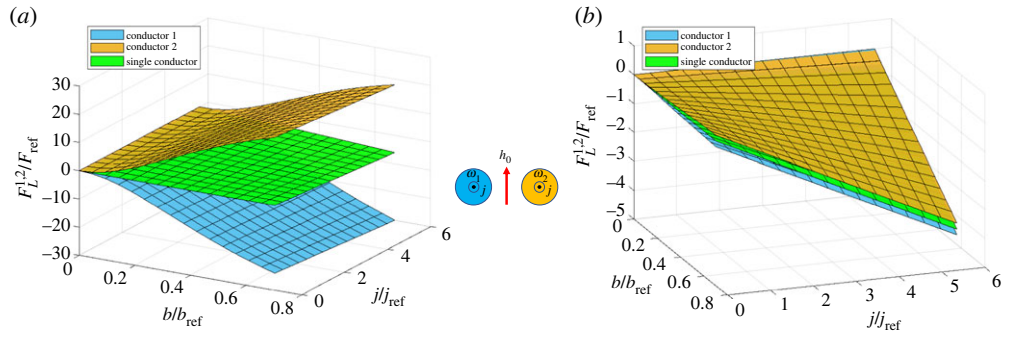

Figure 10. Dimensionless forces per unit length $F_L^{1,2}/F_{\text{ref}}$ as a function of the remote magnetic field vector b_0/b_{ref} and the current density j/j_{ref} on two conductors with equal, same direction parallel currents $I = \pi jR^2$; in (*a*) at distance $D/R = 4$ and in (*b*) at distance $D/R = 20$. Lorentz force for the single conductor $-b_0 l/F_{\text{ref}}$ depicted in green for comparison. (*a*) $F_L^{1,2}/F_{\text{ref}}$ versus $(b_0/b_{\text{ref}}, j/j_{\text{ref}})$ for $D/R = 4.0$, (*b*) $F_L^{1,2}/F_{\text{ref}}$ versus $(b_0/b_{\text{ref}}, j/j_{\text{ref}})$ for $D/R = 20.0$.

As expected from figure 8 where the highest value of the magnetic field for the near-linear magnetic regime loading occurs on the right end of the conductor's cross section, the highest value of the normal components of the magnetic stress also occur in the same location, as depicted in figure 9*a*,*c*. For the high magnetic field and current, again as expected from the results in figure 8, the normal components of the magnetic stress are uniform over the entire conductor: $\overset{m}{\sigma}_{xx}/\mu_0 m_s^2 = 0.30$ in figure 9*d* and $\overset{m}{\sigma}_{yy}/\mu_0 m_s^2 = 0.68$ in figure 9*f*.

Note also that the dimensionless shear component of the magnetic stress is significantly lower inside the conductor compared with its magnitude outside for both loadings: three orders of magnitude lower order in figure 9*b* (3×10^{-12} versus 3×10^{-9}), and two orders of magnitude lower order in figure 9*e* (3×10^{-3} versus 3×10^{-1}). The maximum normal magnetic stresses occur always inside the conductor. By contrast, the maximum magnetic shear stress always occurs on the outside of the conductor's boundary and is the shear component of the Maxwell stress in vacuum. Note also the rotated by $\pm\pi/4$ two symmetry axes of the shear stress fields when compared with the unique symmetry x-axis for the normal ones.

(b) Two conductors under magnetic field and same direction electric currents

We continue with the investigation of the Lorentz forces on two parallel ferromagnetic conductors of circular section of radius R, subjected to parallel currents of the same, uniform current density $\boldsymbol{j} = j\boldsymbol{e}_z$ and a remote external magnetic field vector of magnitude $\boldsymbol{b}_0 = b_0\boldsymbol{e}_y$ (see geometry in figure 5). The results are presented in figures 10 and 11 in dimensionless form, according to (4.1). Of interest is the influence of the conductor's magnetic properties on the Lorentz forces per unit length as a function of their distance D. It is expected that for the closely spaced case ($D/R = 4$), the conductor's magnetic properties will be strongly influencing these forces, while for larger separation distances ($D/R = 20$) this influence will be considerably reduced, as these forces approach $\boldsymbol{F}_L^{1,2} = -b_0 I\boldsymbol{e}_x$ (plane coloured in green and depicted for comparison purposes in figure 10). More specifically, in figure 10*a*, we present the dimensionless forces per unit length $F_L^{1,2}/F_{\text{ref}}$ as a function of the remote magnetic field vector b_0/b_{ref} and the current density j/j_{ref} for $D/R = 4$ and in figure 10*b* for $D/R = 20$.

As expected from $(2.35)_1$, the forces on each conductor have different absolute values. For the closely spaced conductors $D/R = 4$ in figure 10*a*, note that in the absence of current ($j = 0$)[13] the Lorentz forces have opposite signs as expected for two adjacent magnetic dipoles with the same

[13]In the absence of an external magnetic field vector ($b_0 = 0$), the maximum value of the dimensionless Lorentz forces ($F_L^{1,2}/F_{\text{ref}} \approx \pm\mu_0 I^2/2\pi DF_{\text{ref}}$) is negligible—of the order of 10^{-3}—and hence not perceptible at the scale of the plots in figure 10.

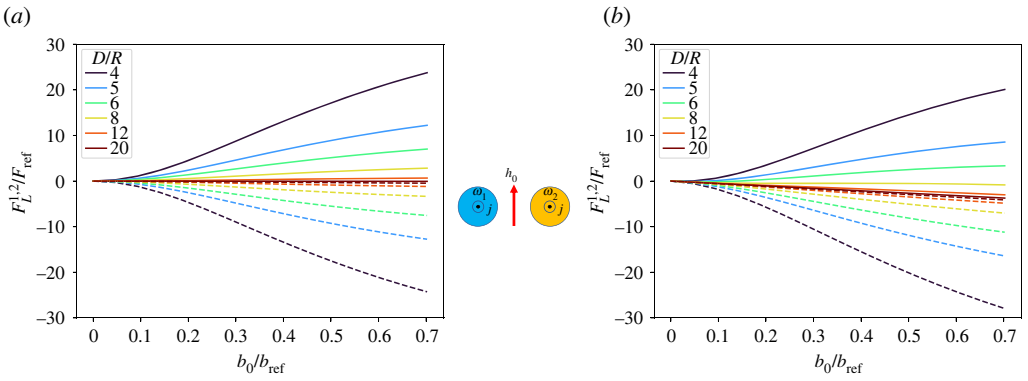

Figure 11. Influence of distance D/R on the dimensionless force per unit length $F_L^{1,2}/F_{\text{ref}}$ between two conductors with equal, same direction parallel currents $I = \pi jR^2$ as a function of the remote magnetic field vector b_0/b_{ref} at two different current densities; in (*a*) for $j/j_{\text{ref}} = 0.42$ and in (*b*) for $j/j_{\text{ref}} = 6.36$. Results for conductor 1 (left) are plotted in dashed lines while for conductor 2 (right) are plotted in solid lines (figure 5). (*a*) $F_L^{1,2}/F_{\text{ref}}$ versus b_0/b_{ref} for $j/j_{\text{ref}} = 0.42$, $4 \leq D/R \leq 20$, (*b*) $F_L^{1,2}/F_{\text{ref}}$ versus b_0/b_{ref} for $j/j_{\text{ref}} = 6.36$, $4 \leq D/R \leq 20$.

orientation; the forces increase in magnitude with increasing magnetic field vector b_0. As the electric currents increase, for a given external magnetic field, the Lorentz forces are only slightly affected, since the magnetic field is dominated by the magnetic properties of the conductor.

For the remotely spaced conductors $D/R = 20$ in figure 10*b* note that the Lorentz forces are an order of magnitude lower than their counterparts in figure 10*a*. Although of different sign in the absence of currents (dipole repulsion), the Lorentz forces in the two conductors eventually share the same sign as the currents increase and converge to the single conductor limit $-b_0 I$, as one can observe in figure 10*b*. It is also worth mentioning at this point that the average between two Lorentz forces is independent of the conductors' magnetic properties, since from $(2.35)_1$ one has that $(F_L^1 + F_L^2)/2 = -b_0 I$.

We can thus conclude that for the closely spaced conductors in figure 10*a* the Lorentz forces are dominated by the dipole repulsion effect due to the conductors' magnetic behaviour, while for the remotely spaced conductors in figure 10*b*, the Lorentz forces are practically unaffected by it. The influence of distance on the Lorentz forces per unit length for two identical parallel ferromagnetic conductors of circular section, subjected to currents of the same direction, as a function of the applied remote external magnetic field vector b_0, and for different distances D/R, is presented in figure 11. The results for conductor 1 (left) are plotted in dashed lines, while for conductor 2 (right) they are plotted in solid lines. More specifically, figure 11*a* corresponds to a low current density $j/j_{\text{ref}} = 0.42$ while figure 11*b* corresponds to a high current density $j/j_{\text{ref}} = 6.36$.

By comparing figure 11*a*,*b*, one can conclude that the ferromagnetic response of the conductors dominates the Lorentz forces, for the close distance and low current density case, while for the same distance an increase in the current density reduces these forces for conductor 1 and increases them for conductor 2. As the conductor distance increases, for a given external magnetic field both forces are significantly decreased, act in the same direction and converge to their common limit $F_L^1 = F_L^2 = -b_0 I$. The dominant factor influencing the Lorentz forces is the magnetic response of the conductor (hence the marked nonlinearity of the force-magnetic field curves for low values of D) and not the magnitude of the current, as evidenced by the results in figure 11.

(c) Two conductors under magnetic field and opposite direction electric currents

Next follows the investigation of the Lorentz forces on two parallel ferromagnetic conductors of circular section of radius R, subjected to parallel currents of the opposite direction, with a

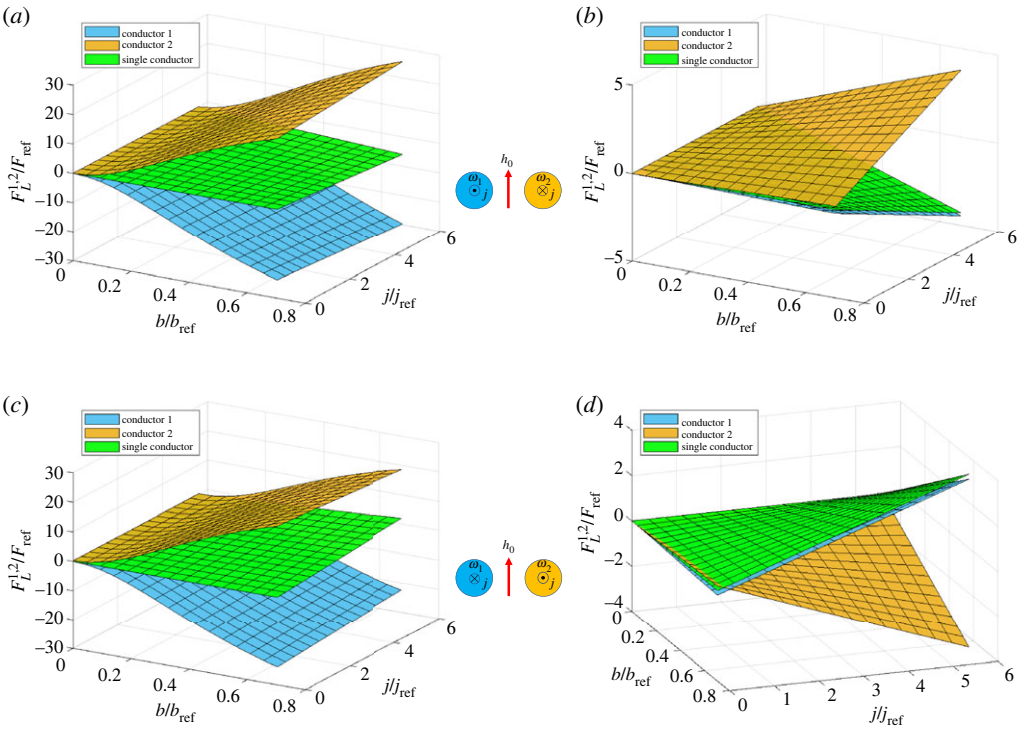

Figure 12. Dimensionless forces per unit length $F_L^{1,2}/F_{\text{ref}}$ as a function of the remote magnetic field vector b_0/b_{ref} and the current density j/j_{ref} on two conductors with equal, opposite direction parallel currents $I = \pi jR^2$ for $j_1 = je_z, j_2 = -je_z$ (case i, (*a*) and (*b*)) and $j_1 = -je_z, j_2 = je_z$ (case ii, (*c*) and (*d*)); in (*a*) and (*c*) at distance $D/R = 4$ and in (*b*) and (*d*) at distance $D/R = 20$. Lorentz force for the single conductor $-b_0 l/F_{\text{ref}}$ depicted in green for comparison. (*a*) $F_L^{1,2}/F_{\text{ref}}$ versus $(b_0/b_{\text{ref}}, j/j_{\text{ref}})$ for $D/R = 4.0$, (*b*) $F_L^{1,2}/F_{\text{ref}}$ versus $(b_0/b_{\text{ref}}, j/j_{\text{ref}})$ for $D/R = 20.0$, (*c*) $F_L^{1,2}/F_{\text{ref}}$ versus $(b_0/b_{\text{ref}}, j/j_{\text{ref}})$ for $D/R = 4.0$, (*d*) $F_L^{1,2}/F_{\text{ref}}$ versus $(b_0/b_{\text{ref}}, j/j_{\text{ref}})$ for $D/R = 20.0$.

uniform current density and a remote external magnetic field vector of magnitude $\boldsymbol{b}_0 = b_0\boldsymbol{e}_y$, as depicted in figure 5. Two possibilities exist: $\boldsymbol{j}_1 = j\boldsymbol{e}_z, \boldsymbol{j}_2 = -j\boldsymbol{e}_z$ (case i) and $\boldsymbol{j}_1 = -j\boldsymbol{e}_z, \boldsymbol{j}_2 = j\boldsymbol{e}_z$ (case ii). The results are presented in figures 12 and 13 in dimensionless form according to (4.1). Of interest again is the influence of magnetic properties on the Lorentz forces per unit length on each conductor as a function of their distance D. More specifically, in figure 12*a*,*c*, we present the dimensionless forces per unit length $F_L^{1,2}/F_{\text{ref}}$ for cases (i) and (ii), respectively, as a function of the remote magnetic field: b_0/b_{ref} and the current density: j/j_{ref} for $D/R = 4$ and in figures 12*b*,*d* their counterparts for $D/R = 20$.

As expected from $(2.35)_2$, the forces on the two conductors always have opposite signs but the same absolute value. For the closely spaced conductors $D/R = 4$ in figure 12*a*,*c*, note that in the absence of current $(j = 0)$[14] the Lorentz forces due to the interaction of two adjacent magnetic dipoles with the same orientation are the same as in figure 10. As the electric currents increase, for a given external magnetic field, the Lorentz forces are only slightly affected since the magnetic field vector is dominated by the magnetic properties of the conductor.

For the remotely spaced conductors $D/R = 20$ in figure 12*b*,*d*, the Lorentz forces are an order of magnitude smaller than their counterparts in figure 12*a*,*c*. Moreover, these forces show very small sensitivity to the conductors' magnetic behaviour, as one can observe in figure 12*b*,*d*. Moreover, in comparing the last two figures note that the change of the current direction in each conductor results in a change of the sign of the Lorentz force. We can thus conclude, like in the parallel

[14]For no external magnetic field vector ($b_0 = 0$), see the remark in figure 13.

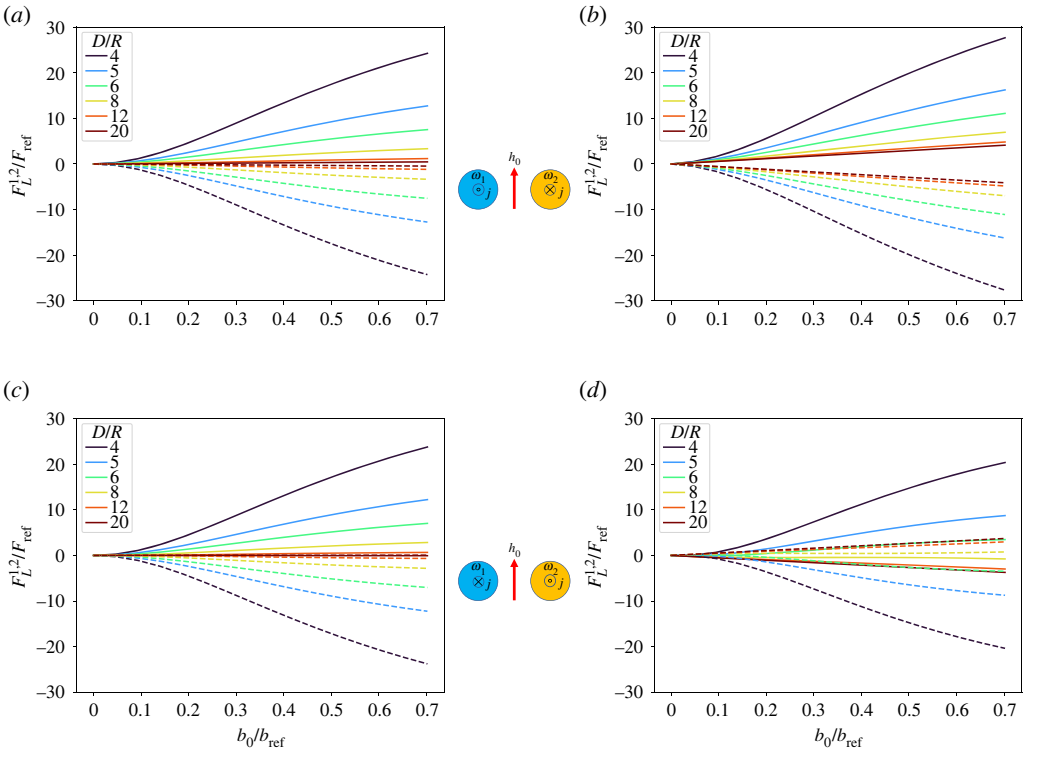

Figure 13. Influence of distance D/R on the dimensionless force per unit length $F_L^{1,2}/F_{\text{ref}}$ between two conductors with equal, opposite direction parallel currents $I = \pi jR^2$ for $j_1 = je_z, j_2 = -je_z$ (case i, (*a*) and (*b*)) and $j_1 = -je_z, j_2 = je_z$ (case ii, (*c*) and (*d*)) as a function of the remote magnetic field vector b_0/b_{ref} at two different densities; in (*a*) and (*c*) for $j/j_{\text{ref}} = 0.42$ and in (*b*) and (*d*) for $j/j_{\text{ref}} = 6.36$. Results for conductor 1 (left) are plotted in dashed lines while for conductor 2 (right) they are plotted in solid lines (figure 5). (*a*) $F_L^{1,2}/F_{\text{ref}}$ versus b_0/b_{ref} for $j/j_{\text{ref}} = 0.42$, $4 \leq D/R \leq 20$, (*b*) $F_L^{1,2}/F_{\text{ref}}$ versus b_0/b_{ref} for $j/j_{\text{ref}} = 6.36$, $4 \leq D/R \leq 20$, (*c*) $F_L^{1,2}/F_{\text{ref}}$ versus b_0/b_{ref} for $j/j_{\text{ref}} = 0.42$, $4 \leq D/R \leq 20$, (*d*) $F_L^{1,2}/F_{\text{ref}}$ versus b_0/b_{ref} for $j/j_{\text{ref}} = 6.36$, $4 \leq D/R \leq 20$.

current direction case, that for the closely spaced conductors in figure 12*a*,*c* the Lorentz forces are dominated by the dipole repulsion effect due to the conductors' magnetic behaviour while for the remotely spaced conductors in figure 12*b*,*d* the Lorentz forces are close to the single conductor limit $\pm b_0 I$, i.e. practically unaffected by magnetic properties.

The influence of distance on the Lorentz forces per unit length for two identical parallel ferromagnetic conductors of circular section, subjected to currents of the opposite direction, as a function of the applied remote external magnetic field vector b_0, and for different distances D/R, is presented in figure 13. The results for conductor 1 (left) are plotted in dashed lines while for conductor 2 (right) they are plotted in solid lines. More specifically, figure 13*a*,*c* for cases (i) and (ii), respectively, correspond to a low current density $j/j_{\text{ref}} = 0.42$, while figure 13*b*,*d* for cases (i) and (ii), respectively, correspond to a high current density $j/j_{\text{ref}} = 6.36$.

By comparing figure 13*a*–*d*, one observes that the ferromagnetic response of the conductors dominates the Lorentz forces for the closely spaced case. Due to this dominance of the magnetic properties for the closely spaced conductors, by comparing figure 13*a*,*c*, we observe that for the low current density, reversing of the current direction has no observable effect on the Lorentz forces. As the conductor distance increases the (always opposite direction) forces converge to the same absolute value (non-ferromagnetic) limit $b_0 I$.

However, the change of the current direction has a noticeable effect for the high current density, as one can observe by comparing figure 13*b*,*d*. According to figure 13*d*, the absolute value of

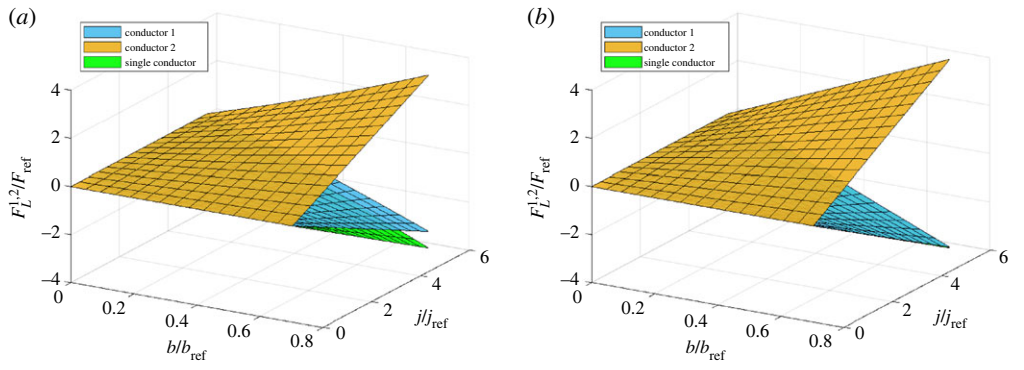

Figure 14. Dimensionless forces per unit length $F_L^{1,2}/F_{\text{ref}}$ as a function of the remote magnetic field vector b_0/b_{ref} and current density j/j_{ref} in an infinite array of equally spaced conductors with alternating direction parallel currents $I = \pi jR^2$; in (*a*) at distance $D/R = 4$ and in (*b*) at distance $D/R = 20$. Lorentz force for the single conductor $-b_0 l/F_{\text{ref}}$ depicted in green for comparison. (*a*) $F_L^{1,2}/F_{\text{ref}}$ versus $(b_0/b_{\text{ref}}, j/j_{\text{ref}})$ for $D/R = 4.0$, (*b*) $F_L^{1,2}/F_{\text{ref}}$ versus $(b_0/b_{\text{ref}}, j/j_{\text{ref}})$ for $D/R = 20.0$.

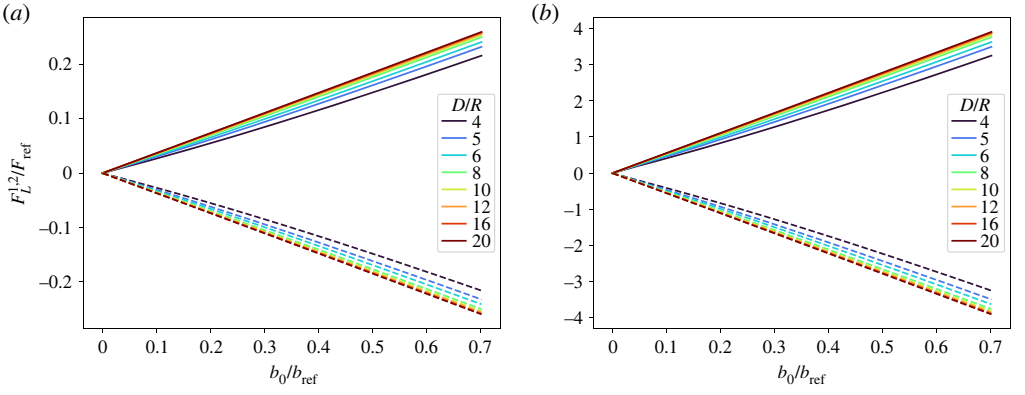

Figure 15. Influence of distance D/R on the dimensionless force $F_L^{1,2}/F_{\text{ref}}$ between two adjacent conductors in an infinite array with alternating direction parallel currents $I = \pi jR^2$ as a function of the remote magnetic field vector b_0/b_{ref} at two different current densities; in (*a*), for $j/j_{\text{ref}} = 0.42$ and in (*b*), for $j/j_{\text{ref}} = 6.36$. Results for conductor 1 (left) are plotted in dashed lines while for conductor 2 (right) they are plotted in solid lines (figure 6). (*a*) $F_L^{1,2}/F_{\text{ref}}$ versus b_0/b_{ref} for $j/j_{\text{ref}} = 0.42$ and $4 \leq D/R \leq 20$, (*b*) $F_L^{1,2}/F_{\text{ref}}$ versus b_0/b_{ref} for $j/j_{\text{ref}} = 6.36$ and $4 \leq D/R \leq 20$.

the forces are significantly lower for case (ii) where they eventually change sign as the distance between the conductors increases, while as seen for case (i) in figure 13*b* the Lorentz forces in each conductor are always of the same sign.

(d) Periodic array of conductors under magnetic field and alternating directions electric currents

We conclude with the investigation of the Lorentz forces on a parallel array of equally spaced ferromagnetic conductors of circular section of radius R, subjected to the same magnitude currents in alternating directions, with a uniform current density $\boldsymbol{j} = \pm j\boldsymbol{e}_z$ and a remote external magnetic field vector of magnitude $\boldsymbol{b}_0 = b_0\boldsymbol{e}_y$, as depicted in figure 6. The results are presented in figures 14 and 15 in dimensionless form according to (4.1).

Of interest, once again is the influence of magnetic properties on the Lorentz forces per unit length on each conductor as a function of their distance D. More specifically in figure 14*a*, we present the dimensionless forces per unit length $F_L^{1,2}/F_{\text{ref}}$ as a function of the remote magnetic field: b_0/b_{ref} and the current density: j/j_{ref} for $D/R = 4$ and in figure 14*b* for $D/R = 20$.

Unlike for the two conductors presented in §4b,c, in the absence of electric currents ($j = 0$), symmetry dictates the Lorentz forces in each conductor to vanish for any value of the external magnetic field, as one can observe in figure 14. In addition, the Lorentz forces for the two different conductor spacings are of the same order of magnitude. Moreover, for given current density and magnetic field, the Lorentz forces are smaller for the more closely spaced conductors $D/R = 4$ than for their more remote counterpart $D/R = 20$, as one can see by comparing figure 14*a*,*b*. The presence of magnetization in the conductor has the counterintuitive effect of weakening the Lorentz forces. Moreover, these forces are almost linearly dependent on the magnetic field and current, as seen from the almost flat surfaces in figure 14. The influence of distance on the Lorentz forces per unit length for a parallel array of equally spaced ferromagnetic conductors of circular section of radius R, subjected to the same magnitude parallel currents in alternating directions, as a function of the applied remote external magnetic field vector b_0, and for different distances D/R, is presented in figure 15. The results for conductor 1 are plotted in dashed lines while those for conductor 2 are plotted in solid lines. More specifically, figure 15*a* corresponds to a low current density $j/j_{\text{ref}} = 0.42$ while figure 15*b* corresponds to a high current density $j/j_{\text{ref}} = 6.36$. The significant current density increase dictated the different scales for plotting the Lorentz forces in figure 15*a*,*b*.

By comparing figures 11 and 13 with 15, one can draw two conclusions. The first is that the magnetic properties of the conductors have considerably less influence on the Lorentz forces in the periodic arrangement, as evidenced by the almost linear force versus magnetic field response which is rather insensitive to the distance between conductors: difference with the non-magnetic case ranging from 18% for $D/R = 4$ and rapidly decreasing to 3% for $D/R = 10$. The second conclusion is the counterintuitive result of an increasing force as the distance between conductors increases, a result of the repulsive dipole–dipole interaction magnetization-induced forces that decrease with increasing distance between conductors. Observe that figures 11 and 13 are plotted at a different scale than figure 15, due to the significant reduction in the Lorentz forces for the periodic conductor case.

5. Conclusion

Although the magnetostatics (i.e. when all field quantities are time-independent) problem of Lorentz forces on electrical current-carrying conductors subjected to a remote magnetic field is a classical one, the impact of the conductors' magnetic properties on the forces between two or more (in a periodic array) parallel conductors subjected to a uniform external magnetic field and current density has not been the subject of investigations to the best of the authors' knowledge, thus motivating the present study.

As discussed in §2d, the calculation of Lorentz forces requires solely the determination of the Maxwell stresses in vacuum, i.e. the magnetic field vector $\boldsymbol{b}$ outside the conductors. Consequently, the continuum two-dimensional numerical calculations (FEM) are considerably simplified for this small strain multiphysics problem, since they involve only the scalar magnetic vector potential $a(x, y)$ (recall $\boldsymbol{a} = a(x, y)\boldsymbol{e}_z$).

The case of two closely spaced conductors $D/R = 4$ is particularly interesting, since the magnetic fields outside the conductors are strongly influenced by the magnetic constitutive law and the resulting magnetic dipole repulsion between the two conductors far outweighs the current-induced forces, as one can see in figures 11 and 13. At large distances $D/R = 20$, the Lorentz forces reduce to the classical result of a single wire in a uniform magnetic field ($F_L^{1,2} = \pm b_0 I$). One can thus significantly increase the Lorentz forces in two closely spaced parallel conductors by using ferromagnetic materials.

The results for an infinite array of parallel, equally spaced conductors are rather surprising, if not counterintuitive. For currents in the same direction, the conductors' magnetic properties have no influence on the Lorentz forces due to geometric symmetry arguments. For the case of currents in alternating directions, the magnetic properties of the conductors only slightly reduce the Lorentz forces due to dipole interactions and these forces are essentially linearly dependent on both the magnetic field and applied current, as attested by the flat surfaces results in figure 14 and the straight lines in figure 15. More complicated, multilayer arrays of conductors can be analysed in exactly the same manner as the single layer array considered here.

The results of this investigation pertain to unsupported conductors surrounded by vacuum, which in view of the linear momentum equation (2.20) will induce motion, as an acceleration term results from the Lorentz forces. When the conductors are imbedded in a non-conducting elastomeric matrix, mechanical tractions appear on the conductors' boundaries and the fully coupled mechanical-electromagnetic problem in §2 must be solved to obtain both the magnetic field vector $\boldsymbol{b}$ and the displacement field $\boldsymbol{u}$. From this equilibrium solution, one finds the elastic stresses $\overset{e}{\boldsymbol{\sigma}}$ inside the conductors as in [11]. Moreover, composites consisting of ferromagnetic materials inside a soft elastomeric matrix have attracted particular attention in recent years (e.g. [5,19,22]), although no electrical currents were considered. The finite strain formulation in §2 is the appropriate modelling tool for an upcoming investigation following the current work.

Data accessibility. This article has no additional data.

Declaration of AI use. We have not used AI-assisted technologies in creating this article.

Authors' contributions. G.M.: conceptualization, formal analysis, investigation, methodology, software, validation, visualization, writing—review and editing; E.C.: supervision, writing—review and editing; N.T.: conceptualization, formal analysis, investigation, methodology, project administration, resources, supervision, validation, visualization, writing—original draft, writing—review and editing.

All authors gave final approval for publication and agreed to be held accountable for the work performed therein.

Conflict of interest declaration. We declare we have no competing interests.

Funding. No funding has been received for this article.

Acknowledgements. This work is part of the PhD thesis of G. Magda, who gratefully acknowledges the support of the Direction Générale de l'Armement.

References

1. Lowes FJ. 1973 Force on a wire in a magnetic field. *Nature* **246**, 208–209. (doi:10.1038/246208a0)
2. Casperson LW. 2002 Forces on permeable conductors in magnetic fields. *Am. J. Phys.* **70**, 163–168. (doi:10.1119/1.1424265)
3. Raposo V, Garcia J, González J, Vázquez M. 2000 Long-range magnetostatic interactions in arrays of nanowires. *J. Magn. Magn. Mater.* **222**, 227–232. (doi:10.1016/S0304-8853(00)00563-1)
4. Hammer JH, Ryutov DD. 1999 Linear stability of an accelerated, current carrying wire array. *Phys. Plasmas* **6**, 3302–3315. (doi:10.1063/1.873598)
5. Liu L, Kuo HY. 2012 Closed-form solutions to the effective properties of fibrous magnetoelectric composites and their applications. *Int. J. Solids Struct.* **49**, 3055–3062. (doi:10.1016/j.ijsolstr.2012.06.007)
6. Kankanala S, Triantafyllidis N. 2004 On finitely strained magnetorheological elastomers. *J. Mech. Phys. Solids* **52**, 2869–2908. (doi:10.1016/j.jmps.2004.04.007)
7. Thomas J, Triantafyllidis N. 2009 On electromagnetic forming processes in finitely strained solids: theory and examples. *J. Mech. Phys. Solids* **57**, 1391–1416. (doi:10.1016/j.jmps.2009.04.004)
8. McDonald KT. 2003 Methods of calculating forces on rigid magnetic media. (http://arxiv.org/abs/physics/0312027).
9. Hanappier N. 2021 Coupled electro-magneto-thermo-mechanical modeling of electric motors. PhD thesis. Ecole Polytechnique.
10. Hanappier N, Charkaluk E, Triantafyllidis N. 2021 A coupled electromagnetic–thermomechanical approach for the modeling of electric motors. *J. Mech. Phys. Solids* **149**, 104315. (doi:10.1016/j.jmps.2021.104315)

11. Hanappier N, Charkaluk E, Triantafyllidis N. 2022 Multiphysics simulation of electric motors with an application to stators. *Intl. J. Solids Struct.* **253**, 111406. (doi:10.1016/j.ijsolstr.2021.111406)
12. Kovetz A. 2000 *Electromagnetic theory*, vol. **975**. Oxford, UK: Oxford University Press.
13. Lax M, Nelson DF. 1976 Maxwell equations in material form. *Phys. Rev. B* **13**, 1777–1784. (doi:10.1103/PhysRevB.13.1777)
14. Perevertov O. 2017 Influence of the applied elastic tensile and compressive stress on the hysteresis curves of Fe-3% Si non-oriented steel. *J. Magn. Magn. Mater.* **428**, 223–228. (doi:10.1016/j.jmmm.2016.12.040)
15. Lopez S, Cassoret B, Brudny JF, Lefebvre L, Vincent JN. 2009 Grain oriented steel assembly characterization for the development of high efficiency ac rotating electrical machines. *IEEE Trans. Magn.* **45**, 4161–4164. (doi:10.1109/TMAG.2009.2023243)
16. Baudouin P, Belhadj A, Breaban F, Deffontaine A, Houbaert Y. 2002 Effects of laser and mechanical cutting modes on the magnetic properties of low and medium Si content nonoriented electrical steels. *IEEE Trans. Magn.* **38**, 3213–3215. (doi:10.1109/TMAG.2002.802418)
17. Pearson J, Squire P, Maylin M, Gore J. 2000 Biaxial stress effects on the magnetic properties of pure iron. *IEEE Trans. Magn.* **36**, 3251–3253. (doi:10.1109/20.908758)
18. Bao S, Gu Y, Fu M, Zhang D, Hu S. 2017 Effect of loading speed on the stress-induced magnetic behavior of ferromagnetic steel. *J. Magn. Magn. Mater.* **423**, 191–196. (doi:10.1016/j.jmmm.2016.09.092)
19. Danas K. 2017 Effective response of classical, auxetic and chiral magnetoelastic materials by use of a new variational principle. *J. Mech. Phys. Solids* **105**, 25–53. (doi:10.1016/j.jmps.2017.04.016)
20. Hall EH. 1879 On a new action of the magnet on electric currents. *Am. J. Math.* **2**, 287–292. (doi:10.2307/2369245)
21. Brown WF. 1966 *Magnetoelastic interactions*. New York, NY: Springer.
22. Galipeau E, Ponte-Castaneda P. 2013 Giant field-induced strains in magnetoactive elastomer composites. *Proc. R. Soc. A* **469**, 20130385. (doi:10.1098/rspa.2013.0385)